ASTRONOMY & ASTROPHYSICS
SUPPLEMENT SERIES

FEBRUARY **1997**, PAGE 255

Astron. Astrophys. Suppl. Ser. **121,** 255-274 (1997)

Ammonia observations towards molecular and optical outflows

G. Anglada[1,2], I. Sepúlveda[1], and J.F. Gómez[3,4]

[1] Departament d'Astronomia i Meteorologia, Universitat de Barcelona, Av. Diagonal 647, E-08028 Barcelona, Spain
[2] Instituto de Astronomía, UNAM, Apdo. Postal 70-264, 04510 México DF, Mexico
[3] Laboratorio de Astrofísica Espacial y Física Fundamental, INTA, Apdo. Correos 50727, E-28080 Madrid, Spain
[4] Instituto de Astrofísica de Andalucía, CSIC, Apdo. Correos 3004, C/ Sancho Panza s/n, E-18080 Granada, Spain

Received February 14; accepted May 20, 1996

Abstract. We observed the $(J,K) = (1,1)$ and $(J,K) = (2,2)$ inversion transitions of the NH_3 molecule towards several regions with molecular or optical outflows: RNO 43, HH 83, HH 84, HH 86/87/88, L1641-N, L100, L483, L673, IRAS 20188+3928, L1228, L1048, HHL 73, L1251 (IRAS 22343 + 7501 and IRAS 22376+7455) and L1262, using the 37 m radio telescope of the Haystack Observatory. Additionally, we searched for the $6_{16}-5_{23}$ H_2O maser line towards nine regions, detecting a weak H_2O maser near IRAS 20188+3928. We detected and mapped NH_3 emission in 14 of the 15 regions observed, and we estimated physical parameters for the high density gas. We systematically found that the position of the best candidate for the outflow excitation in each region is very close to an NH_3 emission peak. From a statistical study of the data presented in this paper, together with previously published data, we conclude that the NH_3 line emission is more intense towards molecular outflow sources than towards sources with only optical outflows. Therefore, molecular outflows appear to be associated with larger amounts of high density gas. This result suggests a possible evolutive scheme in which young objects associated with molecular outflows lose progressively their neighboring high-density gas, weakening both the NH_3 emission and the molecular outflow in the process, and making optical jets more easily detectable as the total amount of gas decreases.

Key words: ISM: jets and outflows — ISM: molecules — masers — stars: formation

1. Introduction

The early stages of stellar evolution are dominated by processes involving strong mass loss. The effect of this mass outflow on nearby molecular cloud material is evidenced principally by the presence, in the radio domain, of molecular outflows and, in the optical domain, by the presence of Herbig-Haro objects and highly collimated jets. Several lines of evidence indicate that molecular outflow is one of the earliest observable phases of the stellar evolution (e.g., Rodríguez 1990). Likewise, Eiroa et al. (1994a) and Persi et al. (1994) concluded that an important fraction of what are thought to be the youngest objects (the so-called Class 0 sources; André et al. 1993) are associated with Herbig-Haro objects, suggesting that not only the molecular outflows but also the optical ones start in the early stages of the star formation process.

One of the remaining open questions regarding the outflow phenomenon is that of the driving mechanism of molecular outflows. There is a growing belief that highly collimated (moving at high velocity; $\gtrsim 100$ km s^{-1}) circumstellar ($\sim 10^4$ AU) optical jets drive the less collimated (and of lower velocity; $\gtrsim 10$ km s^{-1}) molecular outflows that extend to larger, interstellar scales ($\sim 10^5$ AU). Detailed models have been developed in this line (see, e.g., Raga et al. 1993 and references therein). In these "unified models", a high velocity, collimated wind (which would correspond to the optically detected HH objects or jets) drives an envelope of slower, less collimated material (e.g., environmental material set into motion by viscous coupling), which is identified with the molecular outflow. Within this scenario, both optical and molecular outflows would coexist during the pre-main-sequence stages. Despite this coevality, depending on the evolutionary stage of a particular young stellar object, observations could appear dominated by either type of mass loss phenomenon. For the youngest objects, which are still deeply embedded in high density molecular material, circumstellar optical jets are expected to be highly extinguished and hardly detectable, while molecular outflows can be more prominent. As the object evolves, the ambient molecular gas is progressively being swept up by the outflow, and the driving

Send offprint requests to: G. Anglada

jet becomes more easily detectable at optical wavelengths. The decrease of the high density gas near the star is expected to be evidenced through a decrease in the line intensity of high-density tracers, such as the NH_3 molecule.

Another important issue in the outflow study is the identification of the outflow exciting sources. These sources are commonly embedded in high-density gas, and located near the position of the emission maximum of high-density tracers like the NH_3 lines, as shown by Anglada et al. (1989). This association, at a scale $\lesssim 0.1$ pc, between the ammonia emission peak and the outflow exciting source does not contradict the fact that the ammonia emission could present a much smaller scale structure near the object (e.g., cavities), as revealed by very high angular resolution observations (see the discussion by Anglada et al. 1995). Thus, single-dish ammonia observations can be an useful tool to help to establish the position of an outflow exciting source, to confirm a given candidate or to discriminate between several candidates.

In order to further investigate these issues, we selected a sample of 15 star-forming regions with signs of outflow activity, and we mapped with the Haystack 37 m telescope the NH_3 emission around the position of the suspected outflow exciting sources. In this paper we present the results of this study. In Sect. 2 we describe the observations, in Sect. 3 we discuss the sources individually, in Sect. 4 we discuss the global results of our study, and in Sect. 5 we give our conclusions.

2. Observations

The observations were carried out on February 1990 with the 37 m radio telescope at Haystack Observatory[1]. We observed the $(J,K) = (1,1)$ and the $(J,K) = (2,2)$ inversion transitions of the ammonia molecule. At the observing frequencies (23.6944960 GHz and 23.7226320 GHz, respectively), the beam size of the telescope is $1'.4$, and its beam efficiency at an elevation of 45° is ~ 0.35. We used a dual maser receiver and both polarizations were observed. The spectrometer was a 1024-lag digital autocorrelator with an effective bandwidth of 6.67 MHz. The calibration was made with the standard noise-tube method. The observations were made in the position switching mode. All the spectra were corrected for the elevation-dependent gain variations and for atmospheric attenuation. The rms pointing error was estimated to be $\sim 15''$ by observing continuum unresolved sources. System temperature ranged from 70 to 150 K. The data were reduced using the CLASS and GREG packages of IRAM. The observed spectra were smoothed, resulting a velocity resolution of ~ 0.2 km s^{-1}.

We searched 15 sources for $NH_3(1,1)$ emission. In all cases, we first made measurements on a five-point grid centered at the positions given in Table 1, with a full beam separation between points. The $NH_3(1,1)$ line was detected in 14 of these sources. The $NH_3(2,2)$ line was observed in 8 sources, at the positions given in Table 2, and was detected in 6 of them. Spectra of the $NH_3(1,1)$ and $NH_3(2,2)$ lines obtained at the positions given in Table 2 are shown in Figs. 1 and 2, respectively. In Figs. 4 to 13, 15 to 17, and 20, we show the $NH_3(1,1)$ maps of the detected sources.

In Table 2 we give $NH_3(1,1)$ and (2,2) line parameters obtained from a multicomponent fit to the observed spectra at the position of the emission peak, using the CLASS package. In Table 3 we list physical parameters of the high-density cores, derived from the ammonia observations following the procedures explained in the footnotes of the table.

Additionally, we searched for the $6_{16} - 5_{23}$ H_2O maser line (at the observing frequency of 22.235080 GHz) in nine sources. We made five or seven-point maps centered at the positions given in Table 1. For the water maser observations, we used the same spectrometer with the same bandwidth as for the ammonia observations. We reached a typical sensitivity of 1.5 Jy (1σ) per spectral channel. We detected H_2O maser emission towards the region associated with the source IRAS 20188+3928 and the spectrum obtained is shown in Fig. 3. For the other observed sources we do not detect any significant ($> 3\sigma$) H_2O emission.

3. Results for individual sources

3.1. RNO 43

RNO 43 (Cohen 1980) is the brightest spot of a chain of Herbig-Haro knots (Jones et al. 1984; Ray 1987; Mundt et al. 1987) extending $\sim 5'$ to the northeast of the source IRAS 05295 + 1247. This chain is designated as HH 243 in the new catalog of Herbig-Haro objects of Reipurth (1994). Another long ($\sim 5'$), well collimated chain of Herbig-Haro knots (HH 245) extends to the north of RNO 43. Reipurth (1991) found a large fragmented counter bow-shock (HH 244) to the southwest of the IRAS source, suggesting that HH 243 and HH 244 constitute a bipolar HH flow. Anglada et al. (1992) found several radio continuum sources that could be related to the HH 243, HH 244 and HH 245 chains. The high-velocity CO emission in the region has been mapped by Edwards & Snell (1984), Cabrit et al. (1988), and Bence et al. (1996). The CO outflow exhibits a complex distribution with several overlapping red and blueshifted lobes, extending on both sides of the IRAS source, and aligned roughly in the north-south direction. The CO lobes located to the north of the IRAS source were initially proposed to constitute two separate outflows (Edwards & Snell 1984). However, no exciting sources have been found for these proposed outflows. Also, no NH_3 emission associated with these northern lobes has been detected (Anglada et al. 1989). On the other hand,

[1] Radio Astronomy at Haystack Observatory of the Northeast Radio Observatory Corporation is supported by the National Science Foundation.

Table 1. Sources observed in NH_3 or H_2O

Source	Central position		Outflow type[a]	Excitation source[b]	Ref.	NH_3 detected?	NH_3 sensitivity[c] (K)	H_2O detected?	H_2O sensitivity[c] (Jy)
	$\alpha(1950)$	$\delta(1950)$							
IRAS 00213+6530	$00^h21^m22\overset{s}{.}0$	$+65°30'25''$	CO	IRAS	1	-	-	No	1.6
IRAS 00259+6510	$00^h25^m59\overset{s}{.}8$	$+65°10'12''$	CO	IRAS	1	-	-	No	2.4
RNO 43	$05^h29^m32\overset{s}{.}7$	$+12°47'33''$	CO, HH	IRAS	2, 3, 4	Yes	0.03	-	-
HH 83	$05^h31^m06\overset{s}{.}3$	$-06°31'45''$	CO, HH	IRAS	5, 6	Yes	0.03	-	-
HH 84	$05^h31^m44\overset{s}{.}7$	$-06°35'16''$	HH	Hα?	5	Yes	0.04	-	-
HH 86/87/88	$05^h33^m15\overset{s}{.}9$	$-06°38'33''$	HH	?	5	Yes	0.03	-	-
L1641-N	$05^h33^m52\overset{s}{.}7$	$-06°26'02''$	CO	IRAS	7	Yes	0.04	-	-
L100	$17^h13^m03\overset{s}{.}9$	$-20°53'39''$	CO	IRAS	8	Yes	0.05	-	-
L483	$18^h14^m50\overset{s}{.}6$	$-04°40'49''$	CO	IRAS	8	Yes	0.03	-	-
L673	$19^h18^m01\overset{s}{.}3$	$+11°16'27''$	CO	IRAS	9	Yes	0.04	-	-
IRAS 20188+3928	$20^h18^m50\overset{s}{.}7$	$+39°28'18''$	CO	IRAS	10	Yes	0.03	Yes	0.8
L1228	$20^h58^m14\overset{s}{.}5$	$+77°24'05''$	CO, HH	IRAS	11, 12	Yes	0.01	No	1.6
L1048	$21^h33^m24\overset{s}{.}0$	$+50°39'43''$	CO	IRAS	13	No	0.05	-	-
HHL 73	$21^h43^m18\overset{s}{.}0$	$+47°19'00''$	CO, HHL	IRAS	14, 15	Yes	0.03	No	0.8
S140-N	$22^h17^m58\overset{s}{.}1$	$+63°17'50''$	CO, HH	IRAS	16, 17	-	-	No	0.5
IRAS 22343+7501	$22^h34^m22\overset{s}{.}0$	$+75°01'32''$	CO, HH	IRAS	18, 19	Yes	0.03	No	1.6
IRAS 22376+7455	$22^h37^m40\overset{s}{.}8$	$+74°55'50''$	CO, HH	IRAS	18, 20	Yes	0.03	No	1.6
L1262	$23^h23^m48\overset{s}{.}8$	$+74°01'08''$	CO	IRAS	21, 8	Yes	0.04	No	1.6

[a] CO = CO outflow; HH = Herbig-Haro outflow; HHL = Herbig-Haro-like object.
[b] IRAS = IRAS point source; Hα = Hα emission star.
[c] 1-σ rms in the antenna temperature per spectral channel.
References: (1) Fukui 1989; (2) Edwards & Snell 1984; (3) Cabrit et al. 1988; (4) Jones et al. 1984; (5) Reipurth 1989; (6) Bally et al. 1993; (7) Fukui et al. 1988; (8) Parker et al. 1988; (9) Armstrong & Winnewisser 1989; (10) Little et al. 1988; (11) Bally et al. 1995; (12) Haikala & Laureijs 1989; (13) Smith et al. 1989; (14) Dobashi et al. 1993; (15) Gyulbudaghian et al. 1987; (16) Fukui et al. 1986; (17) Eiroa et al. 1993; (18) Sato & Fukui 1989; (19) Balázs et al. 1992; (20) Eiroa et al. 1994b; (21) Terebey et al. 1989.

Cabrit et al. (1988) proposed that the overall high-velocity structure constitutes a single bipolar CO outflow powered by IRAS 05295 + 1247. A CS clump (Cabrit et al. 1988) is associated with the IRAS source. However, the nominal position of the IRAS source appears to be displaced $\sim 1'$ east from the center of the clump. Anglada et al. (1992) found a 3.6 cm VLA source (also detected at 1.3 mm by Reipurth et al. 1993) which is better centered on the CS cloud. Anglada et al. (1992) suggest that the IRAS catalog position is in error by $\sim 30''$ in right ascension, and that the IRAS and the radio continuum sources are tracing the same embedded object, which is the powering source of both the molecular and the HH outflows.

In Fig. 4, we show our NH_3 map of this region. We have detected a weak NH_3 condensation centered $\sim 1'$ to the west of the IRAS source, similar to the CS condensation observed by Cabrit et al. (1988). As the exciting sources of outflows are usually deeply embedded objects, the fact that the high-density gas (traced by the CS and NH_3 emission; Cabrit et al. 1988; this paper) is found associated only with the cm-mm-IRAS source, and that no NH_3 emission was found associated with the northern CO lobes near RNO 43 (Anglada et al. 1989), further supports that the radio continuum source represents a deeply embedded young stellar object, and is the most plausible powering source for the molecular and HH outflows observed in this region, as suggested by Anglada et al. (1992).

3.2. HH 83

This HH object lies at the western edge of the L1641 molecular cloud. The optical structure consists of a jet (at least $32''$ long), apparently emanating from the embedded infrared source HH83 IRS (IRAS 05311 − 0631; Reipurth 1989), which is associated with a reflection nebula and ending with a bow-shock. The jet is highly collimated, and presents large variations in velocity and physical conditions along its length (Reipurth 1989). There is a faint nebulosity $\sim 44''$ southeast of the central infrared source that could be part of the counter bow-shock (Reipurth 1989; Ogura & Walsch 1991). The estimated bolometric luminosity of HH83 IRS is 8 $L_\odot$ (Reipurth et al. 1993). This source does not present detectable radio continuum emission at 3.6 and 2 cm (Rodríguez & Reipurth 1994). Recently, Bally et al. (1994) have mapped a very low velocity, poorly collimated asymmetric molecular outflow (with the redshifted lobe much larger than the blueshifted one) associated with HH83 IRS. These authors suggest

Table 2. NH_3 line parameters[a]

Source	Position[b] (arcmin)	(J,K)	$V_{\rm LSR}$[c] ($\rm km\,s^{-1}$)	$T_{\rm MB}$(m)[d] (K)	ΔV[e] ($\rm km\,s^{-1}$)	$\tau_{\rm m}$[f]	$A\tau_{\rm m}$[g] (K)	$N(J,K)$[h] ($10^{13}\rm cm^{-2}$)
RNO 43	$(-1.4, 0)$	(1,1)	$+10.26 \pm 0.03$	0.46 ± 0.06	0.63 ± 0.07	1.1 ± 0.3	0.80 ± 0.08	1.4
HH 83	(0,0)	(1,1)	$+6.22 \pm 0.05$	0.46 ± 0.06	0.4–0.5	≤ 2[i]	0.6–0.9[j]	0.8–1.1[j]
HH 84	(0,0)	(1,1)	$+8.3 \pm 0.2$	0.3 ± 0.1	1.3–1.5	≤ 3.6[i]	0.3–0.7[j]	1.4–2.5[j]
HH 86/87/88	(1.4,1.4)	(1,1)	$+8.88 \pm 0.03$	0.57 ± 0.06	0.72 ± 0.05	0.1 ± 0.1	0.73 ± 0.04	1.5
L1641-N	$(1.4, -2.8)$	(1,1)	$+6.94 \pm 0.01$	2.7 ± 0.1	0.92 ± 0.03	1.9 ± 0.2	6.0 ± 0.3	15
L100	$(0, 0)$	(1,1)	$+1.64 \pm 0.08$	0.5 ± 0.1	0.4–0.5	≤ 3[i]	0.7–1.3[j]	0.9–1.5[j]
L483	$(0, 0)$	(1,1)	$+5.434 \pm 0.003$	4.54 ± 0.09	0.57 ± 0.01	4.7 ± 0.1	19.9 ± 0.3	32
	$(0, 0)$	(2,2)	$+5.41 \pm 0.03$	0.74 ± 0.06	0.79 ± 0.06	0.2 ± 0.1	0.9 ± 0.4	0.9
L673	$(0, -2.8)$	(1,1)	$+6.94 \pm 0.01$	2.1 ± 0.1	0.49 ± 0.02	1.7 ± 0.3	4.9 ± 0.4	6.7
	$(1.4, 0)$	(2,2)	-	≤ 0.17[k]	-	-	-	-
IRAS 20188+3928	$(0, 0)$	(1,1)	$+1.57 \pm 0.01$	2.66 ± 0.09	1.58 ± 0.02	1.7 ± 0.1	5.3 ± 0.1	23
	$(0, 0)$	(2,2)	$+1.59 \pm 0.02$	1.31 ± 0.06	1.83 ± 0.04	0.5 ± 0.2	1.7 ± 0.3	4.1
L1228	$(0, 0)$	(1,1)	-8.088 ± 0.003	2.71 ± 0.03	0.71 ± 0.01	2.31 ± 0.06	7.0 ± 0.1	14
	$(0, 0)$	(2,2)	-8.06 ± 0.03	0.49 ± 0.6	0.69 ± 0.06	0.2 ± 0.2	0.6 ± 0.1	0.5
HHL 73	$(-2.8, 7)$	(1,1)	$+4.20 \pm 0.01$	1.66 ± 0.09	0.94 ± 0.03	1.8 ± 0.2	3.5 ± 0.2	9.3
	$(-2.8, 7)$	(2,2)	$+4.26 \pm 0.06$	0.31 ± 0.06	0.9 ± 0.1	0.2 ± 0.3	0.4 ± 0.2	0.4
HHL 73	$(8.4, 2.8)$	(1,1)	$+3.74 \pm 0.03$	0.7 ± 0.1	0.67 ± 0.07	3.2 ± 0.3	2.1 ± 0.2	3.9
	$(7, 2.8)$	(2,2)	-	≤ 0.3[k]	-	-	-	-
IRAS 22343+7501	$(1.4, 1.4)$	(1,1)	-4.72 ± 0.02	1.40 ± 0.09	0.56 ± 0.04	1.7 ± 0.4	3.1 ± 0.4	4.8
	$(1.4, 1.4)$	(2,2)	-4.68 ± 0.06	0.23 ± 0.06	0.6 ± 0.1	0.1 ± 0.1	0.3 ± 0.1	0.2
IRAS 22376+7455	$(1.4, 0)$	(1,1)	-3.53 ± 0.01	2.29 ± 0.09	0.69 ± 0.02	1.6 ± 0.2	4.9 ± 0.2	9.3
	$(1.4, 0)$	(2,2)	-3.58 ± 0.04	0.37 ± 0.06	0.8 ± 0.1	0.1 ± 0.2	0.43 ± 0.04	0.5
L1262	$(-1.4, 0)$	(1,1)	$+3.93 \pm 0.01$	1.86 ± 0.09	0.51 ± 0.02	3.6 ± 0.4	6.6 ± 0.5	9.3
	$(0, 0)$	(2,2)	-	≤ 0.17[k]	-	-	-	-

[a] Obtained from a multicomponent fit to the magnetic hyperfine structure, using the CLASS package.
[b] Position of the emission peak (offset from the central position given in Table 1), where line parameters have been obtained.
[c] Velocity of the line with respect to the local standard of rest.
[d] Main beam brightness temperature of the main line of the transition, obtained from a single Gaussian fit.
[e] Intrinsic line width, obtained taking into account optical depth and hyperfine broadening, but not the spectral resolution of the spectrometer.
[f] Optical depth of the main line. For the (1,1) transition, derived from the relative intensities of the magnetic hyperfine components; for the (2,2) transition, derived from the ratio of the (1,1) and (2,2) antenna temperatures and the optical depth of the (1,1) line, assuming the same excitation temperature for both transitions.
[g] Derived from the transfer equation, where $A = f[J(T_{\rm ex}) - J(T_{\rm bg})]$ is the "amplitude" (Pauls et al. 1983), f is the filling factor, $T_{\rm ex}$ the excitation temperature of the transition, $T_{\rm bg}$ the background radiation temperature and $J(T)$ the intensity in units of temperature. Note that $A \simeq fT_{\rm ex}$, for $T_{\rm ex} \gg T_{\rm bg}$.
[h] Beam-averaged column density for the rotational level (J,K), derived from $[N(J,K)/\rm cm^{-2}] = C(J,K)[A\tau_{\rm m}/\rm K][\Delta V/km\,s^{-1}]$, with $C(1,1) = 2.78\ 10^{13}$ and $C(2,2) = 1.31\ 10^{13}$ (e.g., Ungerechts et al. 1986).
[i] Obtained adopting a 3σ upper limit for the intensity of the satellite lines.
[j] The highest value is obtained with the upper limit of $\tau_{\rm m}$, and the lowest value is obtained assuming optically thin emission.
[k] 3σ upper limit.

Table 3. Physical parameters of the NH_3 condensations

Source	Distance (pc)	Ref.	Size[a] (arcmin)	Size[a] (pc)	$T_{\rm rot}^b$ (K)	$N(H_2)^c$ (10^{22} cm^{-2})	M^d ($M_\odot$)	$M_{\rm vir}{}^e$ ($M_\odot$)	$n(H_2)^f$ (10^3 cm^{-3})
RNO 43	400	1	2.6×1.5	0.30×0.18	~ 15	~ 0.4	~ 3	10	~ 1.6
HH 83	470	2	$\gtrsim 2.5 \times 2.3$	$\gtrsim 0.34 \times 0.31$	~ 10	0.4–0.5	$\gtrsim 5$	$\gtrsim 6$	$\gtrsim 1.5$
HH 84	470	2	$\gtrsim 2.6 \times 2.5$	$\gtrsim 0.36 \times 0.34$	~ 11	0.5–1	$\gtrsim 8$	$\gtrsim 66$	$\gtrsim 0.5$
HH 86/87/88	470	2	2.4×1.9	0.33×0.26	~ 19	~ 0.3	~ 4	16	~ 24
L1641-N	480	3	2.3×4.5	0.32×0.63	~ 23	~ 3.5	~ 89	40	~ 5.9
L100	225	4	$\gtrsim 2.3 \times 2.4$	$\gtrsim 0.15 \times 0.16$	~ 12	0.3–0.5	$\gtrsim 1$	$\gtrsim 3$	$\gtrsim 1.1$
L483	200	5	2.0×1.8	0.12×0.10	10	14	21	4	30
L673	300	6	4.7×2.0	0.41×0.18	≤ 12	≥ 2.2	≥ 21	7	≥ 11
IRAS 20188+3928	≤ 4000	7	1.7×2.0	$\leq 1.99 \times 2.33$	18	5.5	≤ 3200	≤ 560	7.3
L1228	300	8	2.9×1.9	0.25×0.17	11	5.3	28	11	13
HHL 73 $(-2.8, 7)$	900	9	2.7×2.0	0.71×0.52	12	3.2	150	56	6.2
HHL 73 $(8.4, 2.8)$	900	9	3.1×2.4	0.81×0.63	≤ 19	≥ 0.9	≥ 59	34	≥ 1.2
IRAS 22343+7501	300	10	3.3×2.0	0.29×0.18	12	1.7	11	8	5.8
IRAS 22376+7455	300	10	7.0×1.8	0.61×0.16	12	3.1	39	16	11
L1262	200	11	2.8×1.7	0.16×0.10	≤ 9	≥ 4.9	≥ 10	3	≥ 8.6

[a] Major and minor axes of the half-power contour of the NH_3 emission.
[b] Rotational temperature, derived from the ratio of NH_3 column density in the (1,1) and (2,2) levels (Table 2) for the sources where the (2,2) line was detected. For the sources undetected in the (2,2) line, an upper limit is obtained assuming that the emission is optically thin. For the sources not observed in the (2,2) line, it is assumed that $T_{\rm ex}({\rm CO}) = T_k = T_{\rm rot}(22-11)$, where the CO data are from Cabrit et al. 1988 (RNO 43), Bally et al. 1993 (HH 83), Morgan & Bally 1991 (HH 84), Maddalena et al. 1986 (HH 86/87/88), Morgan et al. 1991 (L1641-N) and Parker et al. 1988 (L100).
[c] Beam-averaged H_2 column density, obtained from the NH_3 column density in the rotational states given in Table 2, assuming LTE for the metastable rotational states of NH_3 at $T_k = T_R(22-11)$, and an NH_3 abundance $[NH_3/H_2]=10^{-8}$ (see Anglada et al. 1995 for a discussion on NH_3 abundances).
[d] Mass of the condensation, derived from the beam-averaged H_2 column density and the observed area.
[e] Virial mass obtained from $[M_{\rm vir}/M_\odot]=210[R/{\rm pc}][\Delta V/{\rm km\ s^{-1}}]^2$, where R is the radius of the clump, taken as half the geometrical mean of the two linear sizes, and ΔV is the intrinsic line width given in Table 2.
[f] Volume density, derived from the two-level model (Ho & Townes 1983). $T_{\rm ex}$ has been obtained from the values of A given in Table 2, assuming $f = 1$ (this assumption underestimates $T_{\rm ex}$ for unresolved sources).
References.—(1) Maddalena & Morris 1987; (2) Reipurth 1994; (3) Chen et al. 1993; (4) Reipurth & Gee 1986; (5) Ladd et al. 1991a; (6) Herbig & Jones 1983; (7) Little et al. 1988; (8) Bally et al. 1995; (9) Gyulbudaghian et al. 1987; (10) Kun & Prusti 1993; (11) Parker et al. 1991.

that the outflow from HH83 IRS has "blown out" of the molecular cloud and that it may be in a late stage of evolution. Interferometric CS observations (angular resolution $\sim 7''$) of the cloud core associated with HH83 IRS (Nakano et al. 1994) reveal a high-density structure consisting of a bar ($\sim 15''$ long, centered on HH83 IRS and nearly perpendicular to the HH jet) and two ridges surrounding the base of the jet. These authors interpret the CS bar as a rotating circumstellar disk and the two ridges as tracing a small elongated hollow that may be playing an important role in focusing the HH jet.

We have detected a weak NH_3 clump with the emission peak close to the proposed exciting source of HH 83 (see Fig. 5). The NH_3 clump appears unresolved with our beam of $\sim 1\farcm4$, and we cannot study the small scale structure observed in CS by Nakano et al. (1994). At a larger scale, the weakest NH_3 emission seems to extend further to the north and to the west, outside our mapped area. The region we mapped in NH_3 corresponds to the core of the molecular clump studied in ^{13}CO by Bally et al. (1987, 1994), which also shows a clear northern extension.

3.3. HH 84

This HH object was identified and studied by Reipurth (1985, 1989). HH 84 is a long ($\sim 101''$) chain of HH knots outlining a well-collimated optical flow with a position angle of $\sim 154°$. Unlike the large majority of the optical jets, this HH outflow is redshifted with respect to the ambient cloud. Morgan et al. (1991) found evidence for red wing emission in CO profiles, but could not confirm whether this is a molecular outflow. Up to now, no good candidate for the HH flow excitation has been proposed. IRAS 05317−0638 (identified with SW Ori, an Hα star and X-ray source; Strom et al. 1989a) lies $\sim 2'$ south along the jet axis (see Fig. 6). However, based on the morphology of the knots, Reipurth (1989) argues that the flow exciting source should most probably be an embedded source (still undetected) located to the north of the jet.

We found weak ammonia emission associated with the HH knots. Our NH_3 map is presented in Fig. 6. The ammonia emission maximum is close to the northern edge of the jet, and may be tracing the location of a possible embedded exciting source, then supporting the suggestion of

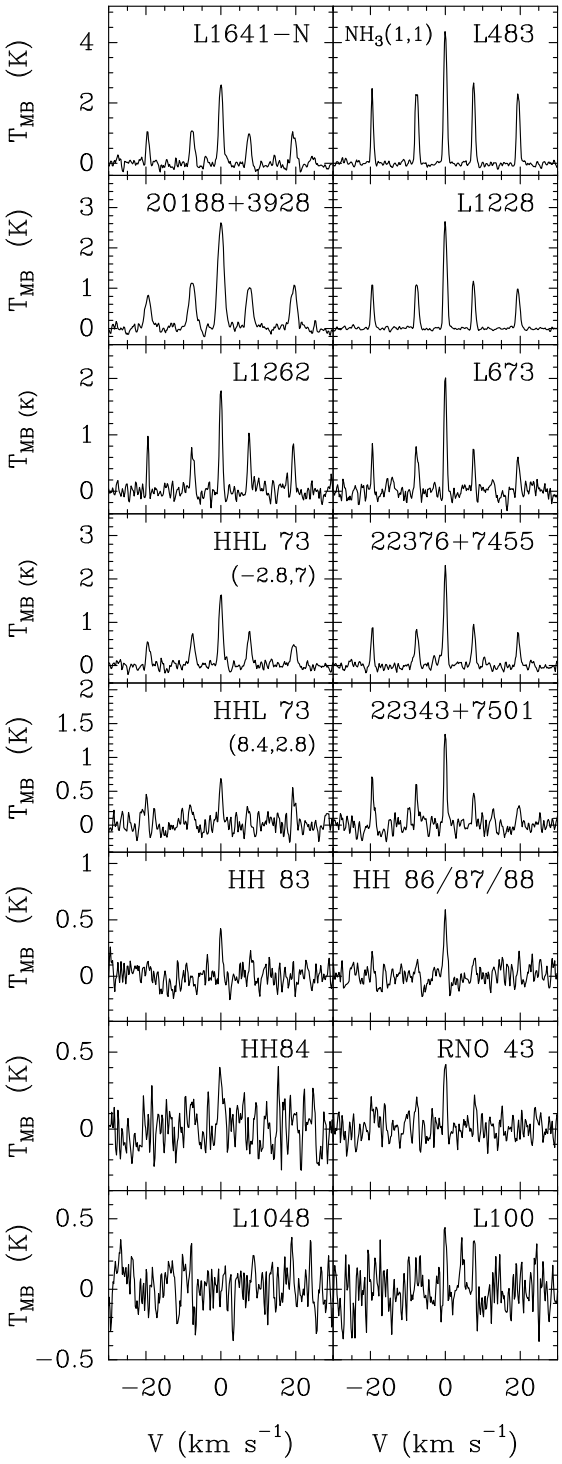

Fig. 1. Spectra of the $(J, K) = (1, 1)$ inversion transition of the NH_3 molecule towards the positions given in Table 2, for the detected sources. The vertical axis is the main beam brightness temperature and the horizontal axis is the velocity with respect to that of the center of the main line (given in Table 2)

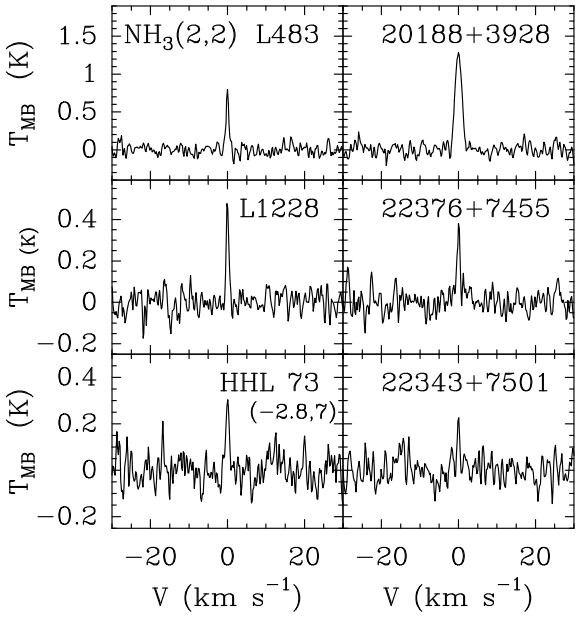

Fig. 2. Same as Fig. 1, for the $(J, K) = (2, 2)$ inversion transition

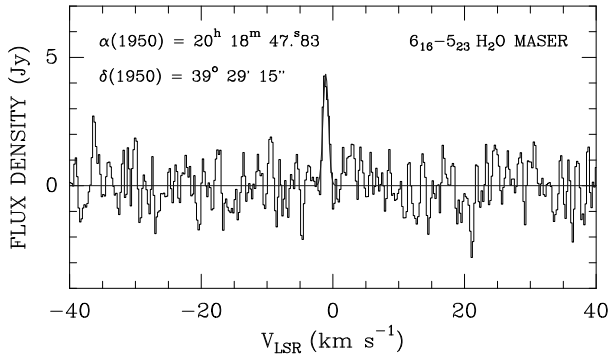

Fig. 3. Spectrum of the H_2O maser detected near IRAS 20188 + 3928, towards the position $\alpha(1950) = 20^h18^m47\overset{s}{.}83$, $\delta(1950) = 39°29'15''$, as observed in Feb. 10, 1990

Reipurth (1989). However, we only mapped a small region and, in particular, our map does not reach the position of the IRAS source. The NH_3 emission appears to extend further to the northeast, roughly following the distribution of the emission of the molecular cloud mapped in ^{13}CO by Bally et al. (1987; see detail in Reipurth 1989).

3.4. HH 86/87/88

The Herbig-Haro objects HH 86, HH 87 and HH 88 appear to be closely associated, and probably originate in the same flow (Reipurth 1985, 1989). The three objects are roughly aligned, but they exhibit a rather complex substructure and no local exciting source has been found. The knots in HH 86 appear to cluster around a faint star, but this star is probably not related to the flow, as

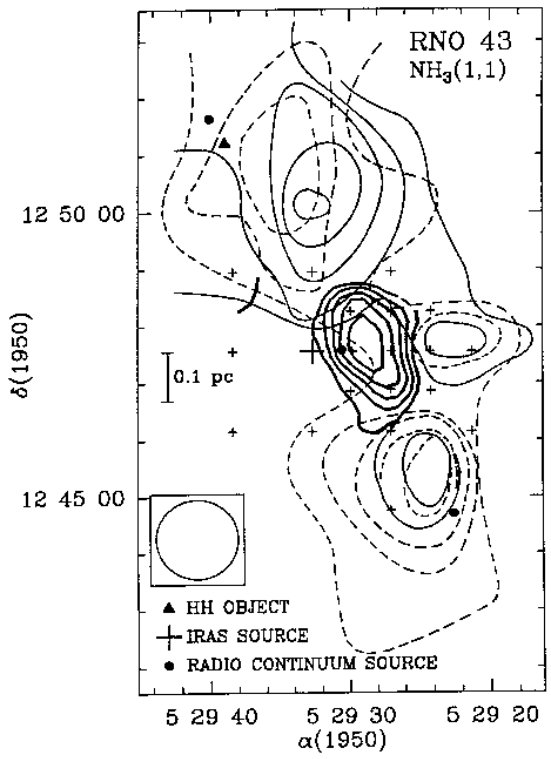

Fig. 4. Contour map of the peak antenna temperature of the main line of the ammonia $(J, K) = (1, 1)$ inversion transition (thick line) in the RNO 43 region. The lowest contour level is 0.1 K, and the increment is 0.02 K. The observed positions are indicated with small crosses. The half power beam width of the telescope is shown as a circle. The positions of several relevant objects in the region are indicated. The central part of the CO bipolar outflow mapped by Cabrit et al. (1988) is shown with thin lines (solid contours indicate blueshifted gas, and dashed contours indicate redshifted gas)

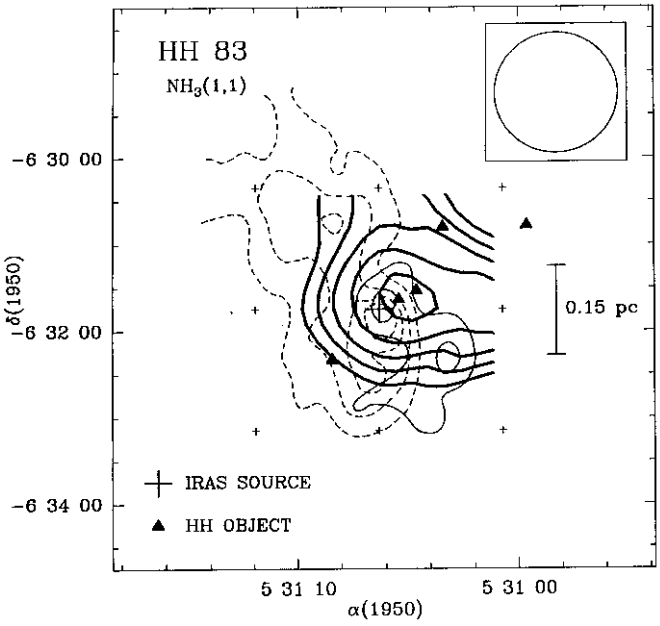

Fig. 5. Same as Fig. 4, for the HH 83 region. The ammonia lowest contour level is 0.08 K, and the increment is 0.02 K. The map of the CO bipolar outflow is from Bally et al. (1994). The position of IRAS 05311 − 0631 is indicated

discussed by Reipurth (1989). The T Tauri star V573 Ori (possibly associated with IRAS 05332−0637; Weintraub 1990) is also close by, but it does not lie on the line traced by the HH jet. Bally & Devine (1994) suggest that these HH objects are the southern end of a 3 pc long "superjet" emanating from the exciting source of HH 34.

Our NH_3 map is shown in Fig. 7. As it can be seen in the figure, the NH_3 emission is faint and displaced to the east of the HH 86/87/88 complex. As the HH 86/87/88 complex lies along a ridge with increasing column density to the east (as mapped in ^{13}CO by Bally et al. 1987), it is plausible that the NH_3 emission continues further to the east of the region we have mapped. Since no NH_3 emission is seen towards the HH complex, this lack of high-density gas associated with the HH objects seems to exclude that their exciting source could be an undetected deeply embedded object in this region, then favoring a non local origin for the HH excitation, as suggested by Bally & Devine (1994).

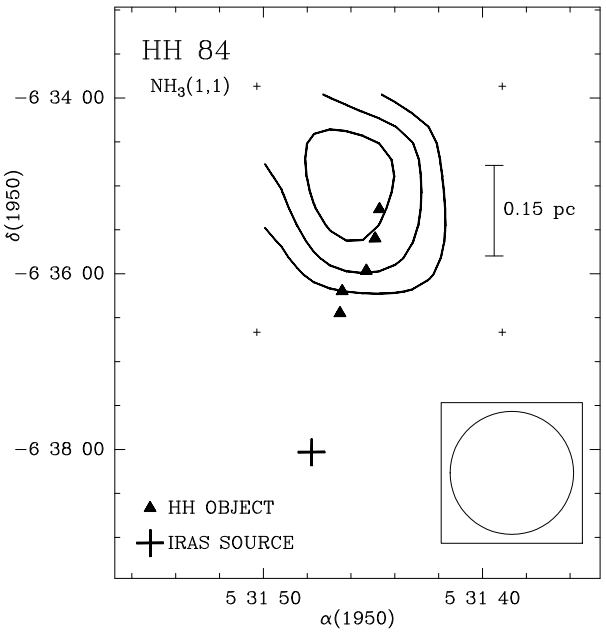

Fig. 6. Same as Fig. 4, for the HH 84 region. The ammonia lowest contour level is 0.08 K, and the increment is 0.02 K. The position of IRAS 05317 − 0638 (identified as SW Ori) is indicated

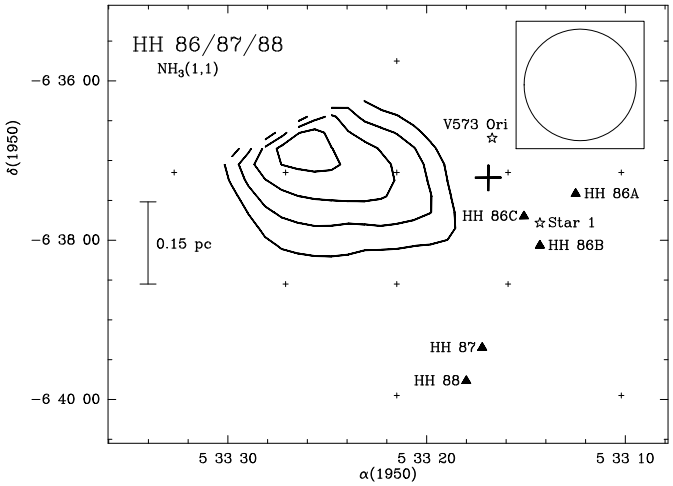

Fig. 7. Same as Fig. 4, for the HH 86/87/88 region. The ammonia lowest contour level is 0.12 K, and the increment is 0.04 K. The position of IRAS 05332−0637 (possibly associated with V573 Ori) is indicated

3.5. L1641-N

A bipolar CO outflow, L1641-N (Fukui et al. 1986, 1988; Wilking et al. 1990), has been mapped in the northern part of the L1641 cloud. The outflow is centered on IRAS 05338−0624, which is proposed as the outflow exciting source. Although optically invisible, this source is one of the most luminous ($L_{\rm IR} \sim 220\ L_\odot$) IRAS sources in this region. Near-IR images (Strom et al. 1989c; Chen et al. 1993) reveal a dense stellar concentration centered on the IRAS position. The IRAS counterpart has been identified in the near-IR (Chen et al. 1993), millimeter (Wilking et al. 1989; Chen et al. 1995) and centimeter (Mundy et al. 1993; Anglada et al. 1996; Chen et al. 1995) ranges. Recently, H_2O maser emission has been found in association with IRAS 05338 − 0624 (Xiang & Turner 1995). In addition, several faint red nebulous objects of unknown nature have been found in a CCD image of the region (Reipurth 1985). A centimeter continuum source (Morgan et al. 1990; Anglada et al. 1996), also visible in the CCD image by Reipurth (1985), is found $\sim 2'$ to the NE of the IRAS source, approximately midway between the red nebulous objects Re 35 and Re 43.

About $3'$ to the SW of the center of the L1641-N molecular outflow, lies the source IRAS 05339−0626. This source ($L_{\rm bol} \sim 86\ L_\odot$) is a typical Class I source (Strom et al. 1989a). Several near-IR sources (Chen et al. 1993) and a centimeter continuum source (Morgan et al. 1990 Anglada et al. 1996) are found near the IRAS position. Red wing CO emission has been observed towards this position, although it is unclear whether this high-velocity emission originates from IRAS 05339−0626 or it is just extended high-velocity emission from the L1641-N outflow (Morgan et al. 1991).

We have mapped in NH_3 a region that includes both IRAS sources. The map we have obtained is shown in Fig. 8. The NH_3 structure consists of two subcondensations, peaking near the positions of the IRAS sources. This result suggests that both IRAS sources are embedded in dense gas. The condensation around IRAS 05338−0624 has been mapped in several molecular species (Fukui et al. 1988; Chen et al. 1992; Harju et al. 1991; McMullin et al. 1994) with the emission peaking close to the IRAS position as in our NH_3 map. In particular, the NH_3 map obtained by Harju et al. (1991) with higher angular resolution ($40''$), is in good agreement with our results. The whole region encompassing both IRAS sources was mapped previously only in HCN (Takaba et al. 1986) and with lower ($\sim 3'$) angular resolution. CS emission was detected but not mapped, towards the two IRAS sources (Morgan & Bally 1991).

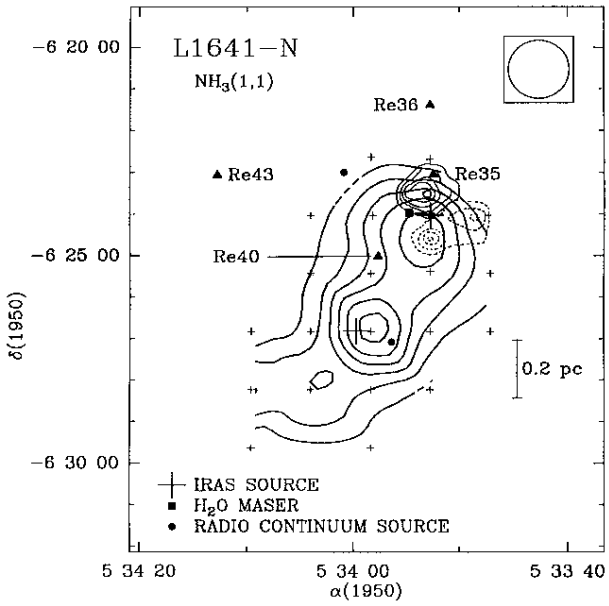

Fig. 8. Same as Fig. 4, for the L1641-N region. The ammonia lowest contour level is 0.15 K, and the increment is 0.15 K. The IRAS source associated with the northern ammonia peak is IRAS 05338−0624 and the one associated with the southern ammonia peak is IRAS 05339 − 0626. The map of the CO outflow is from Fukui et al. (1986)

3.6. L100

L100 (Barnard 62) is a large, very opaque Bok globule in Ophiuchus, surrounded by bright rims. Reipurth & Gee (1986), based on a photometric study, estimate a distance of 225 ± 25 pc. These authors found several Hα emission stars associated with L100 and conclude that IRAS 17130 − 2053 ($0.25\ L_\odot \leq L_{12-100} \leq 0.69\ L_\odot$), an IRAS source with no optical counterpart, represents the

envelope of an embedded PMS object, more evolved than a protostar. Parker et al. (1988) detected a bipolar molecular outflow elongated in the NE-SW direction and centered at the position of IRAS 17130 − 2053, which was proposed as the outflow exciting source.

We have mapped in NH_3 the region around IRAS 17130 − 2053. We have detected faint and unresolved $NH_3(1,1)$ emission peaking near the position of the IRAS source. Our map is shown in Fig. 9. The IRAS position is near the maximum of the ammonia map, in agreement with the idea that it is an object embedded in high-density gas. However, the weakness of the ammonia emission suggests that it is associated with only a small amount of high-density gas and that the size of the ammonia clump could be much smaller than our beam.

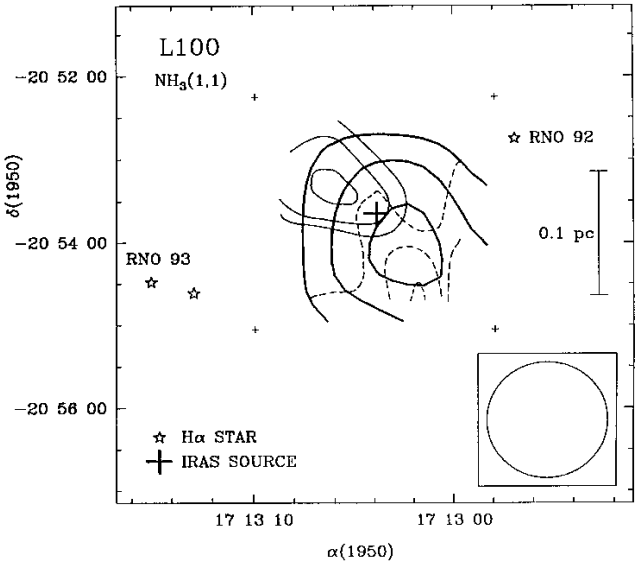

Fig. 9. Same as Fig. 4, for the L100 region. The ammonia lowest contour level is 0.08 K, and the increment is 0.02 K. The map of the CO outflow is from Parker et al. (1988)

3.7. L483

Parker et al. (1988, 1991) and Fuller et al. (1995) have mapped in CO a compact bipolar molecular outflow in the L483 dark cloud. The outflow is clearly elongated along the E-W direction and it is centered on the low-luminosity infrared source IRAS 18148−0440 ($L = 14\ L_{\odot}$, assuming a distance of 200 pc; Ladd et al. 1991a), which is proposed as the outflow exciting source. This source has neither optical nor near-infrared counterpart (Parker 1991). The source has been detected with the VLA at 3.6 cm (Anglada et al. 1996). From the far-IR data and from submillimeter observations (Ladd et al. 1991b; Fuller et al. 1995), Fuller et al. (1995) conclude that the IRAS source is a very young object similar to the so-called Class 0 sources. The source is surrounded by a bipolar near-IR nebula, and a jet-like region of H_2 emission, ending in a bright knot, extends along the blue lobe of the CO outflow (Fuller et al. 1995). An H_2O maser near the IRAS position has been detected by Xiang & Turner (1995) through single-dish observations.

In Fig. 10 we show the ammonia map obtained from our observations. The NH_3 emission peaks very close to the IRAS source position. This fact, together with the infrared results (Fuller et al. 1995), suggest that the IRAS source is deeply embedded in the dense core, giving support to its identification as the powering source of the molecular outflow. Our ammonia map is in good agreement with the ammonia map shown by Fuller & Myers (1993). Fuller & Myers (1993) found two velocity components separated by 0.28 km s^{-1} in an NH_3 spectrum obtained towards the peak of the core, and discuss on their relationship with the overall distribution of dense gas. The velocity resolution of our observations (~ 0.2 km s^{-1}) does not allow us to separate these components in the spectra. Goodman et al. (1993) report a velocity gradient ($\sim 1.9 \pm 0.2$ km s^{-1} pc^{-1}, PA $= 52°$) in the region. From our data, we estimate a velocity gradient of $2 - 3$ km s^{-1} pc^{-1} approximately in the SW-NE direction, which is consistent with the result of Goodman et al. (1993).

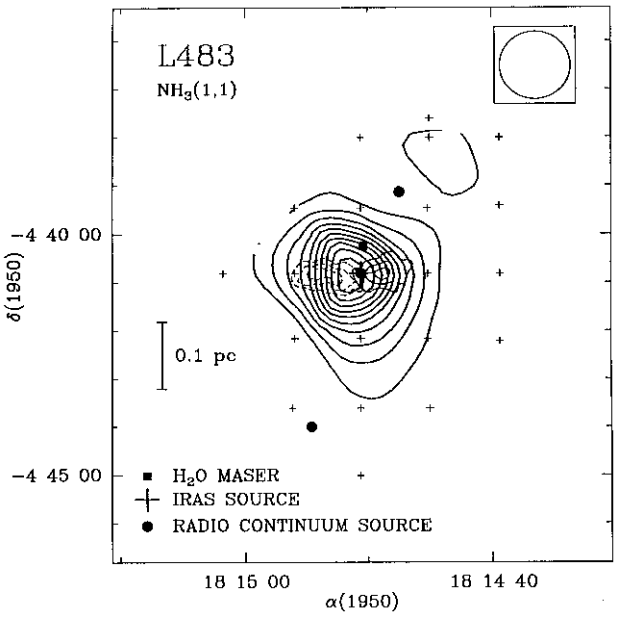

Fig. 10. Same as Fig. 4, for the L483 region. The ammonia lowest contour level is 0.20 K, and the increment is 0.15 K. The map of the CO outflow is from Parker et al. (1988)

3.8. L673

The distance to the L673 dark cloud is not well established. Estimates by different authors range between 150 pc and 400 pc. We will adopt a distance of 300 pc, based on proper motions studies (Herbig & Jones 1983). Armstrong & Winnewisser (1989) discovered a very extended ($10' \times 15'$) bipolar molecular outflow in the northern part of L673. There are four IRAS point sources within five arcmin of the center of the outflow. From an analysis of the IRAS colors, Armstrong & Winnewisser conclude that IRAS 19184+1118 is probably a visible main-sequence star, while the IRAS colors of the other three sources (IRAS 19180 + 1116, 19180 + 1114, 19181 + 1112) are consistent with those of embedded stars. In particular, the source IRAS 19180 + 1116, which coincides with RNO 109 (Cohen 1980), is proposed by Armstrong & Winnewisser (1989) as the most likely candidate to be the outflow exciting source. Ladd et al. (1991a, b) obtained far-infrared photometry and images of IRAS 19180+1116 and IRAS 19180 + 1114, showing that a large fraction of the luminosity of these objects is radiated at long wavelengths ($\lambda > 60$ μm), indicating that they are very young.

Our ammonia map is shown in Fig. 11. The ammonia structure consists of three subcondensations, peaking near the position of the sources IRAS 19180 + 1116 (RNO 109), IRAS 19180 + 1114 and IRAS 19181 + 1112. This result suggests that the three sources are embedded in dense gas. The source IRAS 19180 + 1114 is located very close to the strongest emission maximum, suggesting that this source is associated with the largest amount of high-density gas, being probably the most deeply embedded of these three objects. The spectral energy distribution of this source (Armstrong & Winnewisser 1989; Ladd et al. 1991a) is also consistent with this suggestion. The source IRAS 19180 + 1114 is also well centered in between the two outflow lobes, despite of the irregular geometry of the molecular outflow (see Fig. 11). Taking into account the ammonia results, the spectral energy distribution, and the location with respect to the CO outflow, we favor IRAS 19180+1114 (rather than IRAS 19180+1116 = RNO 109) as the best candidate for the excitation of the molecular outflow in the region.

Although our observations do not reach the position of IRAS 19184 + 1118, from the region we have mapped it seems clear that the NH_3 emission decreases as one moves to the NE, towards the position of this IRAS source. Thus, this source does not appear to be associated with a significant amount of dense molecular gas. This result is confirmed by the CS ($J = 1 \rightarrow 0$) observations of Morata et al. (1996). Even though the CS emission appears to be more extended than the NH_3 emission, the CS map shows that IRAS 19184+1118 lies at the outer edge of the CS distribution, suggesting that this source is not embedded in high density gas. These results are in agreement with those of Armstrong & Winnewisser (1989), which concluded that the IRAS colors of this source are typical of a visible main-sequence star.

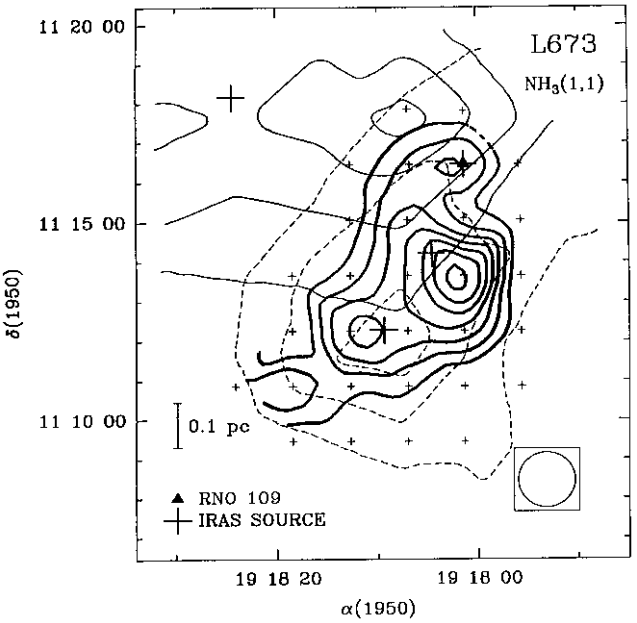

Fig. 11. Same as Fig. 4, for the L673 region. The ammonia lowest contour level is 0.15 K, and the increment is 0.1 K. The IRAS sources associated with the ammonia structure are (from north to south) IRAS 19180 + 1116 (RNO 109), IRAS 19180+1114 and IRAS 19181+1112. The IRAS source outside the ammonia structure is IRAS 19184 + 1118. The map of the CO outflow is from Armstrong & Winnewisser (1989)

3.9. IRAS 20188+3928

IRAS 20188+3928 ($L = 5\ 10^4\ (D/4\ \mathrm{kpc})^2\ L_\odot$; Odenwald & Schwartz 1993) is associated with a compact molecular cloud located in the Cygnus region. The distance to this source is very uncertain (0.4 kpc $\leq D \leq$ 4 kpc; Little et al. 1988). We adopt in this paper its largest value (4 kpc); thus, most of the physical parameters obtained for this region will be upper limits. Little et al. (1988) mapped in ^{12}CO and HCO^+ a bipolar molecular outflow associated with this IRAS source, concluding that the outflowing gas has a dense and clumpy nature.

We have detected a compact ammonia condensation (Fig. 12), with the emission peaking very close to the IRAS 20188 + 3928 position. This result suggests that the IRAS source is deeply embedded in the high density gas, as usually are the exciting sources of molecular outflows. The ammonia lines in this condensation are significantly wider ($\Delta V \sim 1.5 - 2$ km s^{-1}) than in the other regions of our sample (see Table 2). Moreover, there is a north-south velocity gradient in the NH_3 condensation, with the line velocity in the northern part being redshifted (by

$\sim$ 0.5 km s^{-1}) with respect to the southern part, i.e., roughly in the same direction as the outflow. These results suggest that the dense gas around IRAS 20188 + 3928 is perturbed by the outflow from this star and is entrained into the high velocity gas, in agreement with the HCO^+ results obtained by Little et al. (1988).

Palla et al. (1991) detected H_2O maser emission on January 30, 1989 in a single observation towards the position of the IRAS source, obtaining a peak line flux $S_\nu \simeq 45$ Jy and a radial velocity $V_{\rm LSR} = -1.1$ km s^{-1}. We detected this H_2O maser on February 10, 1990. From a seven-point map centered on the IRAS position, we found that the maximum of emission was displaced $\sim 1'$ to the NW of the IRAS source. In Fig. 3, we show the spectrum of the H_2O maser towards this position. The single feature we observed can be fitted with a Gaussian profile having peak line flux $S_\nu = 4.4 \pm 0.9$ Jy, half-power full width $\Delta V = 1.0 \pm 0.1$ km s^{-1}, and radial velocity with respect to the local standard of rest, $V_{\rm LSR} = -1.09 \pm 0.07$ km s^{-1}. Thus, this H_2O maser feature shows high variability on a time scale of one year. Several new maser features, at different velocities appeared also in observations carried out in 1990 and 1991 (Xiang & Turner 1995). One of these features coincides within $4''$ with the position of the IRAS source.

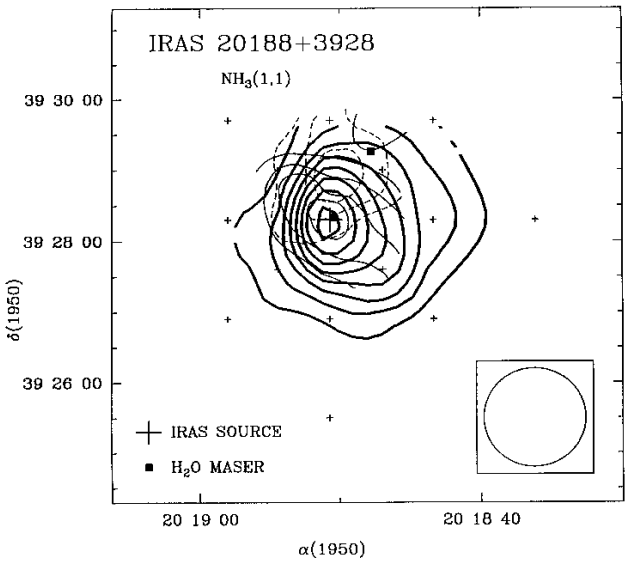

Fig. 12. Same as Fig. 4, for the IRAS 20188+3928 region. The ammonia lowest contour level is 0.20 K, and the increment is 0.1 K. The map of the CO outflow is from Little et al. (1988)

3.10. L1228

L1228 is a high galactic latitude dark cloud, whose distance is poorly known. Haikala et al. (1991) estimate a distance between 100 and 200 pc, while Bally et al. (1995) argue that a better value is 300 pc. In this paper we have adopted this last value. Haikala & Laureijs (1989) discovered a large ($18' \times 9' \simeq 1.6$ pc $\times$ 0.8 pc, for the assumed distance of 300 pc) and well-collimated bipolar CO outflow, with its axis in the NE-SW direction. The outflow is centered on the low luminosity object IRAS 20582 + 7724 ($L \sim 4\ L_\odot$), which was proposed as the outflow exciting source. Anglada et al. (1996) have detected this source in the radio continuum at 3.6 cm with the VLA. Very recently, Bally et al. (1995) have obtained a new CO map of the outflow and detected several HH objects along the axis of the molecular outflow. Moreover, these authors detected an H_2 jet emerging from IRAS 20582 + 7724, but the jet axis differs from that of the molecular outflow by $\sim 40°$, suggesting that the jet ejection direction varies over time. Bally et al. (1995) also detected a long highly collimated HH jet (HH 200), which may be associated with a very low velocity and faint blueshifted CO lobe, and whose exciting source appears to be an embedded T Tauri star located $\sim 1\farcm5$ NW of the IRAS source.

Tafalla et al. (1994) have observed the dense gas around the IRAS source as traced by C_3H_2 and HCN. These authors found sudden shifts in the line velocity of these molecules, with a systematic velocity pattern that agrees in direction and velocity sense with the CO outflow. Tafalla et al. identified three distinct velocity components in the core, and interpreted these results as evidence for the disruption of the dense core by the bipolar outflow from the IRAS source.

Our ammonia map of this region (Fig. 13) shows a condensation of $\sim 3' \times 2'$ in size, elongated in the N-S direction. The ammonia emission peaks very close to the position of the IRAS and radio continuum source, suggesting that this source is deeply embedded in the high density gas, as it is expected for the exciting source of the outflow. For positions with good signal-to-noise ratio, our data show a velocity shift in the ammonia line velocity, consistent with the direction and sense of the bipolar molecular outflow. In Fig. 14 we show the spectra of the NH_3(1,1) main line observed towards the position of the IRAS source, as well as towards two additional positions displaced $1\farcm4$ to the east and $1\farcm4$ to the west, respectively. As it can be seen in the figure, the central velocity of the lines are clearly displaced, with a velocity shift between the extreme positions of $\sim$ 0.54 km s^{-1}, corresponding to a velocity gradient of ~ 2.2 km s^{-1} pc^{-1}. Tafalla et al. (1994), from their higher angular resolution data, obtained velocity gradients of up to 10 km s^{-1} pc^{-1} on a scale of $20''$. Our lower angular resolution data do not allow us to detect these sudden shifts in velocity but, in any case, they provide evidence that the dense gas is perturbed and accelerated by the molecular outflow.

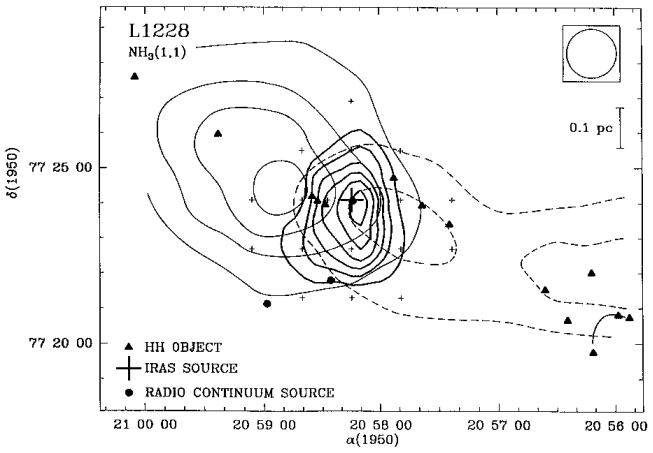

Fig. 13. Same as Fig. 4, for the L1228 region. The ammonia lowest contour level is 0.20 K, and the increment is 0.15 K. The map of the CO bipolar outflow is from Haikala & Laureijs (1989)

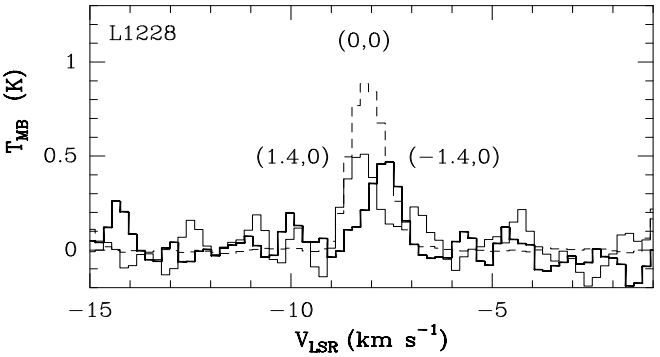

Fig. 14. Spectra of the $NH_3(1,1)$ main line towards three selected positions in L1228. The offsets are in arc minutes with respect to the IRAS position. To make easiest the comparison, the main beam brightness temperature of the (0,0) spectrum has been divided by 3

3.11. HHL 73

HHL 73 is an Herbig-Haro like object, whose position coincides, within observational errors, with an H_2O maser (Gyulbudaghian et al. 1987) and with the source IRAS 21432 + 4719. A region of $\sim 9' \times 7'$ around HHL 73 was mapped in ammonia by Verdes-Montenegro et al. (1989), using also the Haystack radio telescope. Their observations revealed a condensation with an angular size of $\sim 4\farcm7 \times 2\farcm2$, elongated in the NW-SE direction, and with the HHL 73 object located very close to the ammonia emission peak. Verdes-Montenegro et al. (1989) detected also a weaker ammonia condensation, located $\sim 5'$ northeast of the main condensation. No signs of star formation associated with this second clump are known at present.

The region was mapped in CS by Pastor et al. (1991). The CS emitting region is elongated in the E-W direction and it is more extended ($23' \times 7'$) than the region mapped in ammonia by Verdes-Montenegro et al. (1989). The CS structure presents several emission peaks, three of them coinciding with IRAS 21429 + 4726, IRAS 21432 + 4719 and IRAS 21441 + 4722. These IRAS sources have faint optical counterparts on the Palomar Sky Survey red print and were classified as "protostar type" by Dobashi et al. 1992. Recently, Dobashi et al. (1993) have detected three highly asymmetric molecular outflows associated with these IRAS sources.

To complete the study in NH_3 of this region, we carried out new observations, completing those of Verdes-Montenegro et al. (1989), in order to cover the overall region observed in CS. In Fig. 15 we show the complete NH_3 map of the region (including the data of Verdes-Montenegro et al. 1989). Four ammonia clumps, coinciding with emission peaks in the CS map of Pastor et al. (1991), are observed in the figure. Three of the ammonia clumps are associated with an IRAS source, located very close to the emission peak, thus suggesting that these clumps contain a young embedded object. The mean separation between these clumps ($\sim 1 - 2$ pc) is of the order of the typical distance between stars. Therefore, this region appears to be an example of simultaneous formation of several stars in the same cloud, as it was suggested by Pastor et al. (1991).

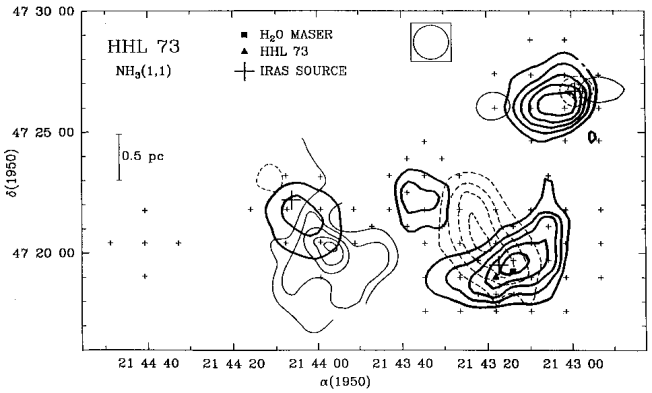

Fig. 15. Same as Fig. 4, for the HHL 73 region. The ammonia lowest contour level is 0.12 K, and the increment is 0.1 K. The NH_3 map obtained by Verdes-Montenegro et al. (1989) is also included. The maps of the CO outflows are from Dobashi et al. (1993)

3.12. L1251

L1251 is an elongated dark cloud (Lynds 1962) apparently belonging to the "Cepheus Flare" giant molecular cloud complex (Lebrun 1986). The estimated distance of this cloud is between 200 pc to 500 pc. We have adopted a distance of 300 pc, estimated from a photometric study by Kun & Prusti (1993). Several indications of low-mass star formation have been found in L1251, with several Hα

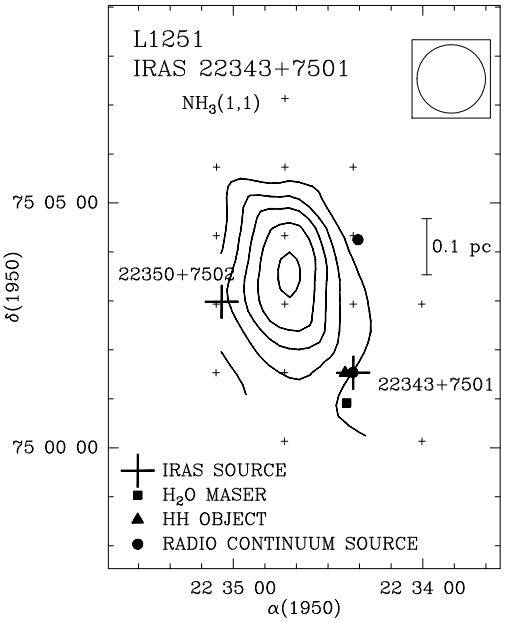

Fig. 16. Same as Fig. 4, for the IRAS 22343 + 7501 region in L1251. The ammonia lowest contour level is 0.1 K, and the increment is 0.1 K

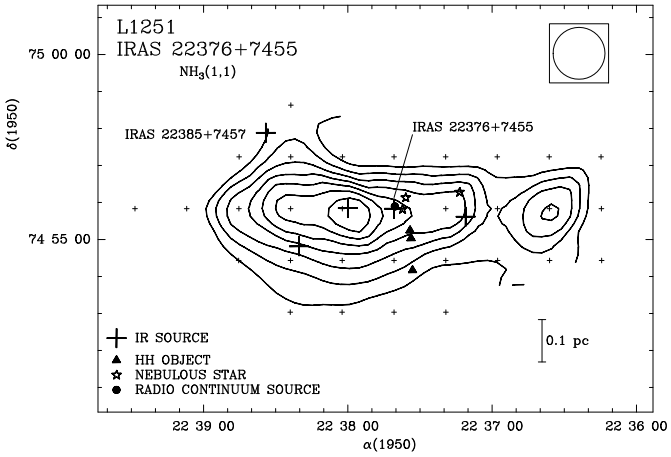

Fig. 17. Same as Fig. 4, for the IRAS 22376 + 7455 region in L1251. The lowest contour level is 0.15 K, and the increment is 0.1 K

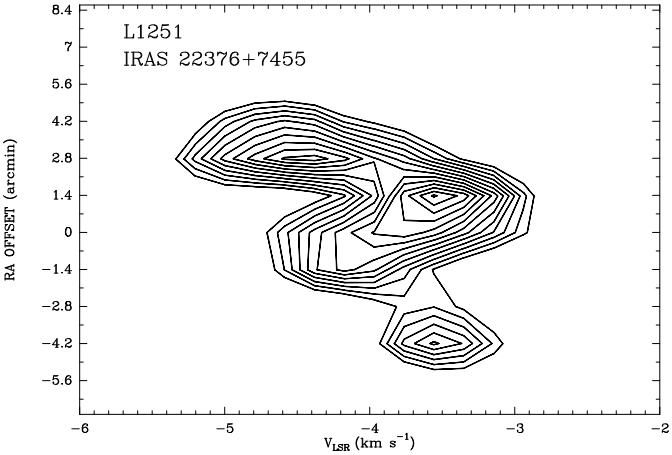

Fig. 18. Position-velocity diagram of the $NH_3(1,1)$ main line along the major axis (PA = 0°) of the condensation associated with IRAS 22376 + 7455, in L1251. The lowest contour level is 0.2 K and the increment is 0.05 K. Right ascension offsets are from the position of IRAS 22376 + 7455

emission stars and infrared point sources detected in the cloud (see Kun & Prusti 1993 and references therein). Our following study of this region focuses on two IRAS sources, IRAS 22343 + 7501 and IRAS 22376 + 7455, which are the most luminous sources in L1251 and appear to be the powering sources of bipolar CO outflows.

3.12.1. IRAS 22343+7501

IRAS 22343+7501 is the driving source of an extended and poorly collimated outflow, L1251-A (Schwartz et al. 1988; Sato & Fukui 1989). The outflow map differs from one study to the other. The outflow map obtained by Sato & Fukui (1989) represents molecular gas with relatively low velocity ($\lesssim$ 4 km s^{-1}) and is extended ($\sim$ 1.1 pc), with the axis approximately in the NE-SW direction. On the other hand, the map obtained by Schwartz et al. (1988), with higher angular resolution, includes higher velocity gas ($\lesssim$ 8 km s^{-1}), is more compact and shows a clear asymmetry in the intensity the two lobes.

Balázs et al. (1992) detected several Herbig-Haro objects (apparently forming an optical jet with its axis coincident with that of the CO outflow), and propose that the exciting source of these objects is also IRAS 22343 + 7501. Anglada et al. (1996) have detected this source in the radio continuum at 3.6 cm. Xiang & Turner (1995) have detected an H_2O maser within $\sim$ 0.′6 of the IRAS position.

The source IRAS 22350 + 7502 (probably a T Tauri star; Kun & Prusti 1993) lies about 2′ to the north-east of IRAS 22343 + 7501.

In Fig. 16, we show our ammonia map. The two IRAS sources lie at the edge of the NH_3 condensation, being displaced by $\sim$ 2′ ($\sim$ 0.1 pc) from the emission peak. At present, no source coincident with the ammonia emission peak has been found. As the emission peak is displaced from the outflow center, it is not likely that the outflow exciting source coincides with this ammonia maximum. The fact that the source proposed as the exciting source of the outflow, IRAS 22343+7501, is displaced $\sim$ 0.1 pc in projection from the ammonia emission peak may be due either because the outflow has disrupted part of the cloud core, or because the source was formed in the dense cloud but has escaped out of the clump (for a velocity of the star with respect to the cloud of $\sim$ 1 km s^{-1}, a time of $\sim 10^5$ yr, which is similar to the time-scale of the outflow,

is required to cover the observed displacement). We note that Morata et al. (1996) have mapped this region in CS, obtaining that the CS extends over a region larger than the NH_3 with IRAS 22343+7501 near a CS emission peak.

3.12.2. IRAS 22376 + 7455

CO observations in the region associated with this source (Sato & Fukui 1989; Sato et al. 1994) have revealed a well collimated and very compact bipolar outflow, L1251-B, extending over $4'$ in the NW-SE direction. IRAS 22376 + 7455 ($L_{\rm FIR} = 14\ L_\odot$; Sato et al. 1994) lies near the center of the two lobes, suggesting that is driving the bipolar outflow. IRAS 22376 + 7455, apparently without optical counterpart (Kun & Prusti 1993; Eiroa et al. 1994b), is detected in the radio continuum at 3.6 cm by Anglada et al. (1996), and is likely to be a protostar embedded in a dense molecular cloud core (Sato et al. 1994). Eiroa et al. (1994b) found several Herbig-Haro objects (HH 189A, B and C) that may be associated with IRAS 22376 + 7455 or with a nearby nebulous star. Kun & Prusti (1993) and Eiroa et al. (1994b) also found several infrared sources and Hα emission stars in this region.

In Fig. 17 we show our ammonia map. The observed NH_3 condensation appears to be very elongated ($\sim 8' \times 2'$) in the east-west direction. IRAS 22376+7455 is located in the midst of the high density gas, confirming that it is an embedded source. However, this source is displaced $\sim 1'$ ($\sim$ 0.1 pc) from the NH_3 emission peak. Several other infrared sources are observed towards the NH_3 condensation, suggesting that they represent embedded sources. One of these sources coincides positionally with the NH_3 emission peak. There is a secondary emission peak (located $\sim 6'$ to the west of the main one) that appears not to be associated with any known infrared source. The source IRAS 22385 + 7457 is located $\sim 4'$ to the northeast of IRAS 22376 + 7455, at the edge of the NH_3 structure, suggesting that it is not deeply embedded in the dense cloud. This source is associated positionally with an Hα emission star, and it is proposed to be a T Tauri star (Kun & Prusti 1993), in agreement with the suggestion that this source is more evolved than the sources still deeply embedded in dense gas.

From our NH_3 data, we found a velocity gradient of $\sim$ 1.4 km s^{-1} pc^{-1} in the NE-SW direction, with sudden velocity shifts of up to 1 km s^{-1} (corresponding to gradients of 8 km s^{-1} pc^{-1}) along the region. In Fig. 18 we show a position-velocity diagram along the major axis of the clump. The velocity gradient does not follows the NH_3 condensation axis, but it has a complex bidimensional structure, so that we do not think that it is due to a global rotational motion of the dense condensation. Goodman et al. (1993) from NH_3 observations, Morata et al. (1996) from CS observations, and Sato & Fukui (1989) from $C^{18}O$, also found the existence of a velocity gradient in this region.

In Fig. 19, we show the overall L1251 region, enclosing the two ammonia condensations we have mapped and their associated molecular outflows. Note that these two condensations coincide with the two brightest spots in the $C^{18}O$ map by Sato et al. (1994).

3.13. L1262

L1262 is an isolated Bok globule with a very high visual extinction (Lynds 1962) located at a distance of 200 pc (Parker et al. 1991). Parker et al. (1988, 1991) discovered a well-collimated bipolar molecular outflow approximately 2.′5 in extent along its axis. Interferometric ^{12}CO observations (Terebey et al. 1989) show a more compact ($\sim 20''$) outflow. The outflow is elongated in the northeast-southwest direction and is centered at the position of the source IRAS 23238 + 7401, which is proposed as the exciting source of the outflow. This IRAS source has been classified as a Class I embedded source without optical counterpart (Parker 1991). The velocity of the outflow decreases gradually as one moves away from the source (Parker et al. 1988). Anglada et al. (1996) found two radio continuum sources at 3.6 cm, one of them being associated with the IRAS source.

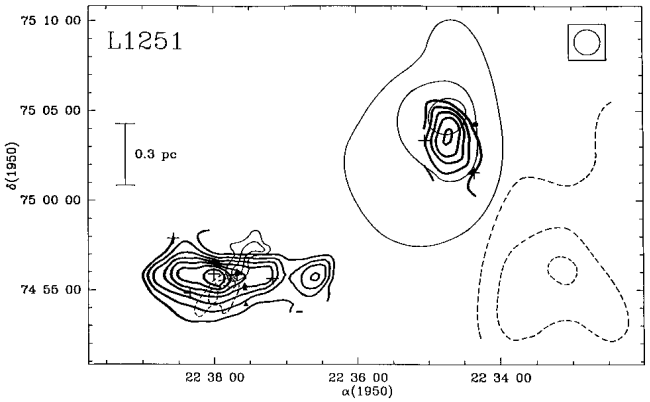

Fig. 19. Region enclosing the two ammonia dense cores observed in L1251 (Figs. 16 and 17). Superposed are shown the two associated CO outflows, L1251-A and L1251-B (Sato et al. 1994)

Our NH_3 map is shown in Fig. 20. The NH_3 condensation presents two emission peaks, one of them coinciding with the source IRAS 23238+7401. Our map is similar to the map obtained by Benson et al. (1984) using the same ammonia inversion line, but our sensitivity is slightly better and we are able to distinguish two emission peaks. Zhou et al. (1989) observed this region in CS, $J = 2 \rightarrow 1$ and $J = 3 \rightarrow 2$, obtaining that the CS emission is more extended than the NH_3 one, as it is usually found in other regions.

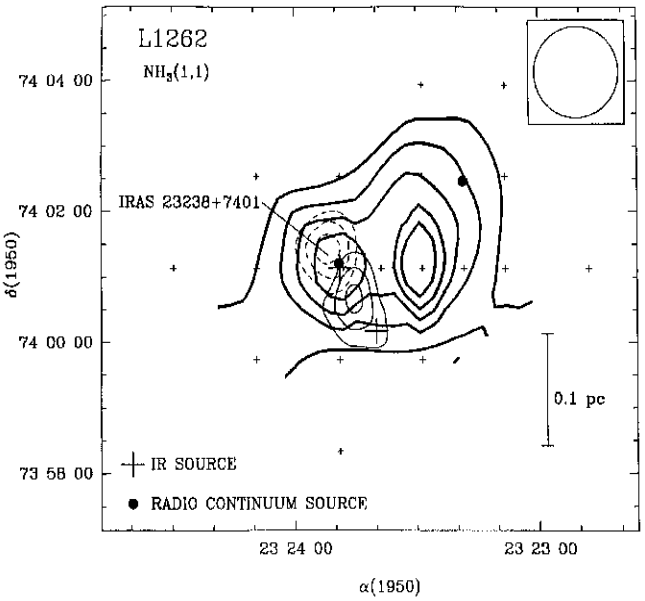

Fig. 20. Same as Fig. 4, for the L1262 region. The ammonia lowest contour level is 0.15 K, and the increment is 0.1 K. The map of the CO outflow is from Yun & Clemens (1994)

4. Discussion

4.1. Location of the exciting sources of the outflows

Through the $(J, K) = (1, 1)$ and (2,2) inversion transitions of the NH_3 molecule we have studied the dense gas in a sample of 15 regions with signs of star formation, as indicated by the presence of outflow activity. We have been able to detect and map the NH_3 emission in 14 of these regions. This high rate of detections is a clear indication of the strong association between NH_3 emission and outflow activity. This result confirms the young nature of the observed objects, since they appear to be still associated with (and most of them embedded in) the dense gas from where they have been formed.

In all cases where we have mapped the NH_3 emission associated with molecular outflows, the ammonia maximum is located near (< 0.1 pc) the position of a candidate for driving the outflow. This result gives support to their identification as the outflow exciting sources, following the criterion proposed by Anglada et al. (1989) for such identification. For the sources of our sample that are only associated with optical signs of outflow, the NH_3 emission is weak and does not coincide with any known object in the observed field, suggesting that probably none of the nearby objects that have been detected up to now is related to the outflow excitation.

4.2. Physical parameters of the dense cores

The sizes of the condensations we have mapped in NH_3 range from ~ 0.1 to ~ 0.8 pc (a somewhat larger value of 2 pc is obtained for the condensation associated with IRAS $20188 + 3928$, but this value may be overestimated by an order of magnitude, since we have adopted the upper limit for the distance). We find evidence for some elongation in the condensations we mapped (as was noted, in general, by Myers et al. 1991). However, our angular resolution, in general, is not good enough to allow us to further discuss on the morphology of the sources. In particular, we are not able to establish whether or not these condensations play a relevant role in the collimation of the outflows in these regions (as suggested, e.g., by Torrelles et al. 1983). We note, however, the very high degree of elongation of the condensation associated with IRAS 22376+7455 in L1251, reminiscent of the NH_3 structure observed in L1448 (e.g., Anglada et al. 1989). In both cases (L1251 and L1448), several objects are seen in projection towards the elongated NH_3 structure. A high angular resolution study of the L1251 region may be relevant in order to investigate a possible fragmentation of the structure. A higher angular resolution study may also be relevant for other sources of our sample that appear unresolved in our present single-dish study.

The intrinsic line widths obtained (~ 1 km s^{-1}; see Table 2) are significantly larger than the expected thermal line widths, since the kinetic temperature estimates for these regions give very low values (see Table 3). Only for the region associated with IRAS $20188 + 3928$ the line widths reach ~ 2 km s^{-1} (in some positions). This is also the region where we have obtained the highest value for the kinetic temperature, as estimated from our ammonia observations (we note that in many sources we only could obtain upper limits or we were forced to use estimates from CO data, which are less accurate). Despite the uncertainty in the distance, the luminosity of IRAS $20188 + 3928$ appears to be higher than for most of the objects studied in our sample. Thus, this object appears to produce a larger perturbation in its molecular high density environment than the others objects we have observed.

In part due to our lack of angular resolution, we are not able to measure in detail the velocity gradient in our regions. However, it is remarkable that in the condensation associated with IRAS $22376 + 7455$ in L1251, our results show the presence of a strong velocity gradient with sudden velocity shifts of up to ~ 1 km s^{-1} between contiguous positions. A study with high angular resolution of this region appears to be very promising.

The H_2 column densities we have obtained are $\sim 10^{22}$ cm^{-2} (assuming $[NH_3/H_2] = 10^{-8}$), implying mean visual extinctions ~ 10 mag. For L483 we have obtained the highest H_2 column density ($\sim 10^{23}$ cm^{-2}, corresponding to a visual extinction of ~ 100 mag), suggesting that this object is very deeply embedded.

The masses obtained for the observed regions lie typically in the range from 1 to 100 $M_\odot$. The values derived coincide, in general, with the virial masses within a factor of 3. This general trend, observed for the regions

of our sample, suggests that the condensations are near virial equilibrium and that the assumed NH_3 abundance is adequate. L483 is the region for which the calculated mass exceeds the virial mass by the largest factor. This could imply that for this source the cloud is still in the process of gravitational collapse. We note here that recently Myers et al. (1995) have detected asymmetric line profiles in this region consistent with infall motion, according to the modeling of Anglada et al. (1987). Although the uncertainties involved are still large, it seems clear that this object is among the youngest sources in our sample, in agreement with the results of Fuller et al. (1995), which classify this as a very young object.

4.3. Evolutive differences in the outflow sources

We have detected and mapped the NH_3 emission in 12 out of 13 regions with molecular outflow in our sample. Only in one region, L1048 (for which, in fact, no published map of the CO outflow is available), we failed in detecting ammonia emission (Table 1). The NH_3 emission is faint ($T_{\rm MB} \lesssim 0.5$ K; see Table 2) only in 3 regions (RNO 43, HH 83 and L100) of the 12 regions associated with molecular outflow we have mapped. On the other hand, in the two regions without molecular outflow (HH 84 and HH 86/87/88), the ammonia emission is very faint. These results tentatively suggest that the ammonia emission tends to be more intense for those sources associated with molecular outflow than for the sources associated with only "optical" signs of outflow (such as jets and Herbig-Haro objects).

In order to substantiate this possible relationship between the type of outflow and the intensity of the NH_3 emission, we have complemented the sample of regions observed in this paper with the results of other Haystack NH_3 observations reported in the literature. We have studied the distribution of the intensity of the NH_3 emission, as measured by the main beam brightness temperature towards the outflow exciting source, in this larger sample of regions. We note here that the NH_3 brightness temperature is a good measure of the intensity of the NH_3 emission only for sources that fill the beam of the telescope. For unresolved sources, a more adequate comparison should be made in terms of the distance corrected flux density of the ammonia emission ("ammonia luminosity"). As we expect that for nearby sources the angular size of the ammonia emission will be, in general, larger than the telescope beam, we have used the main beam brightness temperature to make the comparison, restricting our sample to nearby enough regions. Thus, we have used sources with $D \leq 1$ kpc, and completed our sample with the data from Torrelles et al. (1983) (9 sources), Anglada et al. (1989) (13 sources), Benson & Myers (1989) (5 sources, and 2 additional sources observed at Green Bank), Verdes-Montenegro et al. (1989) (3 sources), and Persi et al. (1994) (1 source).

Our final sample is shown in Table 4. It contains a total of 47 sources, with 21 sources associated only with molecular outflow, 19 sources associated both with optical and molecular outflow and 7 sources with only optical outflow. In Fig. 21 we present the distribution of the NH_3 main beam brightness temperature towards the position of the proposed outflow exciting source (Table 4) for the three groups of sources. The mean values of the NH_3 brightness temperature are 1.7 K (only molecular outflow), 1.5 K (optical and molecular outflow) and 0.5 K (only optical outflow). Despite the relatively small number of sources with only optical outflow, it is clear that these sources tend to present lower values for the NH_3 brightness temperature, while for the sources with molecular outflow the distribution is displaced to higher values of the NH_3 brightness temperature. We conclude, thus, that *the ammonia emission is in general more intense in molecular outflow sources than in sources with optical outflow.*

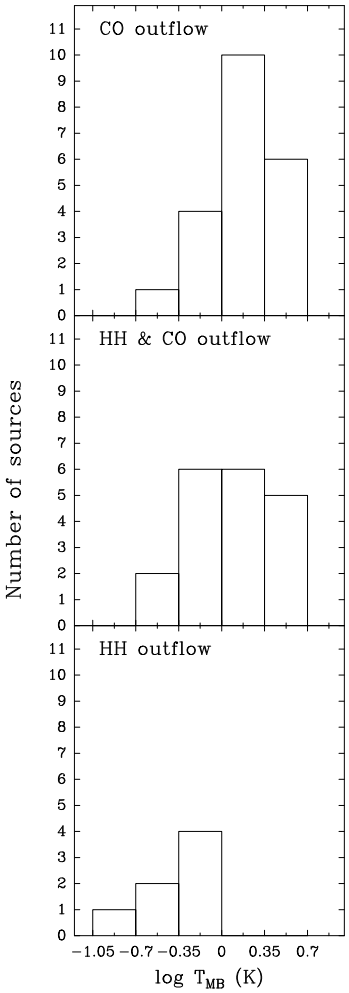

Fig. 21. Distribution of the NH_3 main beam brightness temperature for sources with only molecular outflow (top), for sources with both molecular and optical outflow (middle), and for sources with only optical outflow (bottom)

Table 4. Regions associated with molecular or optical outflow observed in NH_3[a]

Source	Outflow associated	Ref.	T_{MB} (K)	$N(NH_3)$ (10^{14} cm^{-2})	Ref.	D (pc)	Ref.
L1448 (RNO 13)	CO	1	0.3	0.4	2	350	3
L1448N	CO, HH	4, 5	3.1	4	2	350	3
L1448C	CO	4	2.5	3	2	350	3
GL490	CO	6	≤ 0.5	≤ 0.6	7	900	8
L1455	CO	9	2.5	1.6	2	350	3
L1489	CO	10	0.8	4	11	140	8
HH 156	HH	12	≤ 0.6	≤ 0.7	11	140	13
L1524 (Haro 6-10)	HH	14	≤ 0.6	≤ 1	2	140	13
L1551	CO, HH	15, 16	2.72	2.3	7	140	13
HL Tau	CO, HH	17, 18	≤ 1	≤ 1	7	140	13
L1527	CO, HH	19, 20	2.12	5.0	11	140	13
RNO 43 (IRAS 05295+1247)	CO, HH	21, 22	0.40	0.4	23	400	24
HH 83	CO, HH	25, 26	0.46	0.4–0.5	23	470	13
HH 84	HH	25	0.3	0.5–1	23	470	13
HH 33/40	HH	27	≤ 0.3	≤ 0.5	28	470	13
HH 86/87/88	HH	25	≤ 0.2	≤ 0.1	23	470	13
HH 34	CO, HH	29, 30	1.3	≤ 1	2	480	31
L1641-N	CO	32	2.2	2.8	23	480	33
HH 38-43	HH	27	≤ 0.5	≤ 0.6	2	480	31
Haro 4-255 FIR	CO	1	2.2	2.1	2	480	31
B35	CO	10	1.2	4.0	11	500	34
HH 26 IR	CO, HH	35, 36	2.7	2.1	7	470	13
NGC 2071	CO	37	2.44	2.2	7	500	8
Mon R2	CO	38	1.2	1.5	7	800	8
GGD 12-15	CO	39	1.52	2.3	7	1000	8
RMon	CO, HH	40, 35	≤ 0.5	≤ 0.6	7	800	13
NGC 2264	HH	41	≤ 1	≤ 1	2	800	13
HH 120	CO, HH	42, 43	1.8	2.5	44	400	45
L43	CO	1	2.7	2.7	2	160	46
L100	CO	47	0.5	0.3–0.5	23	225	48
L483	CO	47	4.54	14	23	200	49
R CrA	CO, HH	1, 50	2.8	2.0	2	130	51
L673	CO	52	2.1	≥ 2.2	23	300	3
HH 32a	CO, HH	35, 17	≤ 0.6	≤ 0.7	2	300	13
L778	CO	10	1.8	6.3	11	250	8
B335	CO, HH	53, 54	1.2	7.9	11	250	13
L1228	CO, HH	55, 56	2.71	5.3	23	300	56
V1331 Cyg	CO	1	0.5	2.3	2	700	57
L1172	CO	10	1.8	7.9	11	440	8
NGC 7129	CO, HH	58, 59	0.52	0.36	7	1000	13
HHL 73 (IRAS 21429+4729)	CO	60	1.66	3.2	23	900	61
HHL 73 (IRAS 21432+4719)	CO, HHL	60, 61	1.25	1.1	28	900	61
HHL 73 (IRAS 21441+4722)	CO	60	0.7	≥ 0.9	23	900	61
S140N	CO, HH	31, 62	0.88	1.4	28	900	63
L1251 (IRAS 22343+7501)	CO, HH	64, 65	0.29	1.7	23	300	66
L1251 (IRAS 22376+7455)	CO, HH	64, 67	1.71	3.1	23	300	66
L1262	CO	47	1.57	≥ 4.9	23	200	68

[a] Regions with distance ≤ 1 kpc.

References: (1) Levreault 1985; (2) Anglada et al. 1989; (3) Herbig & Jones 1983; (4) Bachiller et al. 1990; (5) Eiroa et al. 1994a; (6) Snell et al. 1984; (7) Torrelles et al. 1983; (8) Fukui et al. 1993; (9) Goldsmith et al. 1984; (10) Myers et al. 1988; (11) Benson & Myers 1989; (12) Strom et al. 1986; (13) Reipurth 1994; (14) Elias 1978; (15) Snell et al. 1980; (16) Mundt & Fried 1983; (17) Edwards & Snell 1982; (18) Mundt et al. 1988; (19) Eiroa et al. 1994a; (20) Heyer et al. 1987; (21) Edwards & Snell 1984; (22) Jones et al. 1984; (23) this paper; (24) Maddalena & Morris 1987; (25) Reipurth 1989; (26) Bally et al. 1994; (27) Haro 1953; (28) Verdes-Montenegro et al. 1989; (29) Haro 1959; (30) Chernin & Masson 1995; (31) Genzel et al. 1981; (32) Fukui et al. 1986; (33) Chen et al. 1993; (34) Felli et al. 1992; (35) Herbig 1974; (36) Snell & Edwards 1982; (37) Bally 1982; (38) Loren 1981; (39) Rodríguez et al. 1982; (40) Cantó et al. 1981; (41) Adams et al. 1979; (42) Cohen & Schwartz 1987; (43) Olberg et al. 1989; (44) Persi et al. 1994; (45) Petterson 1984; (46) Chini 1981; (47) Parker et al. 1988; (48) Reipurth & Gee 1986; (49) Ladd et al. 1991a; (50) Strom et al. 1974; (51) Marraco & Rydgren 1981; (52) Armstrong & Winnewisser 1989; (53) Frerking & Langer 1982; (54) Vrba et al. 1986; (55) Haikala & Laureijs 1989; (56) Bally et al. 1995; (57) Chavarría-K 1981; (58) Loren 1977; (59) Ray et al. 1990; (60) Dobashi et al. 1993; (61) Gyulbudaghian et al. 1987; (62) Eiroa et al. 1993; (63) Crampton & Fisher 1974; (64) Sato & Fukui 1989; (65) Balázs et al. 1992; (66) Kun & Prusti 1993; (67) Eiroa et al. 1994b; (68) Parker et al. 1991.

We should note that recent sensitive studies have detected weak CO outflows in regions where previous studies failed in the detection (e.g., in HH 1-2 or HH 34; Chernin & Masson 1995). We have not attempted to take into account the effect of the intensity of the molecular outflow in our study, and we have only considered whether or not an outflow detection has been reported in a given region.

The fact that the sources of molecular outflow present more intense ammonia emission can be interpreted as indicating that these sources are deeply embedded in the high density gas, and surrounded by a larger amount of molecular gas, while those sources with only optical outflow have already dispersed the molecular core or escaped from it. This interpretation can be corroborated by comparing the estimated column density in the sources listed in Table 4. We found that the ammonia column density towards the outflow exciting source decreases as the outflow activity becomes prominent in the optical. The mean values of the NH_3 column density are 3.3 10^{14} cm^{-2} (only molecular outflow), 2.2 10^{14} cm^{-2} (optical and molecular outflow) and 6.6 10^{13} cm^{-2} (only optical outflow). In Fig. 22 we show the distribution of the NH_3 column density for the three groups of sources. A similar correlation is obtained if the comparison is made in terms of the estimated mass of the associated core, but in this last case it is unclear to what extent should the NH_3 emission be considered as associated with a given object.

These results suggest an evolutive sequence of the sources, traced by the intensity of the ammonia emission and the observational appearance of the outflow. Molecular and optical outflow would be phenomena that dominate, observationally, at different stages of the early stellar evolution. In the younger objects molecular outflows will be prominent, while optical outflows will progressively show up as the star evolves. However, this result does not exclude that both phenomena could coexist simultaneously as is required in the so-called "unified models", in which molecular outflows are driven by highly collimated jets (e.g., Raga et al. 1993); only the observational appearance of the outflow evolves in time as the star loses progressively the surrounding high density gas. In this scenario, the driving optical jet is becoming visible as a consequence of the ambient molecular material being progressively removed by the effect of the molecular outflow itself. Alternatively, the observed differences could represent intrinsic differences in the amount of molecular high density gas from one to another region.

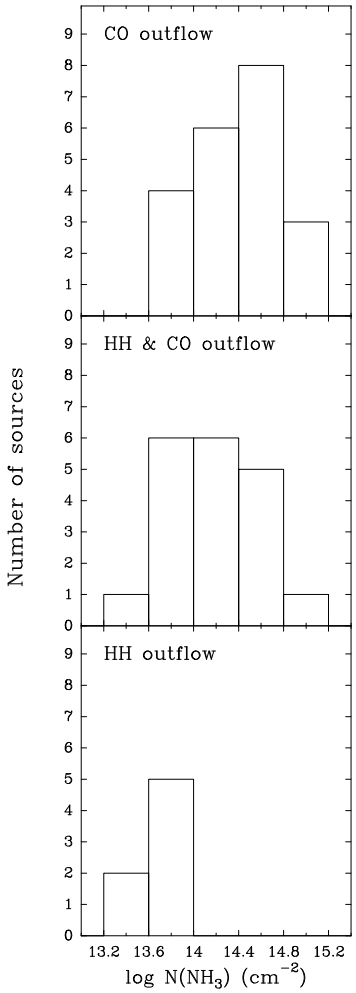

Fig. 22. Distribution of the NH_3 column density for sources with only molecular outflow (top), for sources with both molecular and optical outflow (middle), and for sources with only optical outflow (bottom)

5. Conclusions

We have detected and mapped the ammonia emission in 14 sources of a sample of 15 sources associated with molecular and/or optical outflows. In addition, we have searched for H_2O maser emission towards 9 regions, and detected a weak H_2O maser near IRAS 20188 + 3928. Our main conclusions drawn from this study can be summarized as follows:

1. In all the molecular outflow regions we have mapped, the NH_3 emission peak is very close to the position of a good candidate for the outflow exciting source.
2. For the two regions with only optical outflow (HH 84 and HH 86/87/88), *no* object is detected towards the observed (weak) NH_3 condensations, suggesting a non local origin for the flow excitation.
3. We found that, in general, the NH_3 condensations are very cold, with line widths dominated by non thermal (turbulent) motions. Among the observed sources, IRAS 20188 + 3928 appears to be the object that produces a larger perturbation in its molecular high density environment. Evidence for disruption of the L1228 NH_3 core has also been found.
4. The ammonia condensations appear to be, in general, close to virial equilibrium. L483 is remarkable in

being associated with the largest visual extinction of our sample and being in a possible gravitational collapse, making this source a very good candidate to be a very young deeply embedded object.

5. A very elongated NH_3 structure, apparently associated with several young objects and with strong velocity gradients, has been found near IRAS 22376 + 7455 in L1251.
6. Our main result is the discovery of a correlation between the intensity of the NH_3 emission and the presence of molecular or optical outflow. The NH_3 brightness temperature and column density decrease as the outflow activity becomes prominent in the optical. This result suggests an evolutive scheme in which young objects lose progressively their neighboring high density gas. More NH_3 observations towards the exciting sources of optical jets and HH objects could be very useful to increase the sample in order to allow a more detailed study.

Acknowledgements. We thank the referee, R. Cesaroni, for his careful review of the paper. G.A. and J.F.G. acknowledge support from DGICYT grant PB92-0900, Spain. J.F.G. is also supported by Junta de Andalucía, Spain.

References

Adams M.T., Strom K.M., Strom S.E., 1979, ApJ 230, L183
André P., Ward-Thompson D., Barsony M., 1993, ApJ 406, 122
Anglada G., Rodríguez L.F., Cantó J., Estalella R., López R., 1987, A&A 186, 280
Anglada G., Rodríguez L.F., Torrelles J.M., et al., 1989, ApJ 341, 208
Anglada G., Rodríguez L.F., Cantó J., Estalella R., Torrelles J.M., 1992, ApJ 395, 494
Anglada G., Estalella R., Mauersberger R., et al., 1995, ApJ 443, 682
Anglada G., et al., 1996 (in preparation)
Armstrong J.T., Winnewisser G., 1989, A&A 210, 373
Bachiller R., Cernicharo J., 1986, A&A 168, 262
Bachiller R., Cernicharo J., Martín-Pintado J., Tafalla M., Lazareff B., 1990, A&A 231, 174
Balázs L.G., Eislöffel J., Kelemen J., Kun M., 1992, A&A 255, 281
Bally J., 1982, ApJ 261, 558
Bally J., Devine D., 1994, ApJ 428, L65
Bally J., Langer W.D., Stark A.A., Wilson R.W., 1987, ApJ 312, L45
Bally J., Castets A., Duvert G., 1994, ApJ 423, 310
Bally J., Devine D., Fesen R.A., Lane A.P., 1995, ApJ 454, 345
Bence S.J., Richer J.S., Padman R., 1996, MNRAS (in press)
Benson P.J., Myers P.C., 1989, ApJS 71, 89
Benson P.J., Myers P.C., Wright E.L., 1984, ApJ 279, L27
Cabrit S., Goldsmith P.F., Snell R.L., 1988, ApJ 334, 196
Cantó J., Rodríguez L.F., Barral J.F., Carral P., 1981, ApJ 244, 102
Chavarría-K C., 1981, A&A 101, 105
Chen H., Fukui Y., Yang J., 1992, ApJ 398, 544
Chen H., Tokunaga T., Strom K.M., Hodapp K.-W., 1993, ApJ 407, 639
Chen H., Zhao J.H., Ohashi N., 1995, ApJ 450, L71
Chernin L. M., Masson C.L., 1995, ApJ 443, 181
Chini R., 1981, A&A 99, 346
Cohen M., 1980, AJ 85, 29
Cohen M., Schwartz R.D., 1983, ApJ 265, 877
Cohen M., Schwartz R.D., 1987, ApJ 316, 311
Crampton D., Fisher W.A., 1974, Pub. Dominion Ap. Obs. 14, 283
Curiel S., Raymond J.C., Rodríguez L.F., Cantó J., Moran J.M., 1990, ApJ 365, L85
Dobashi K., Yonekura Y., Mizuno A., Fukui Y., 1992, AJ 104, 1525
Dobashi K., Onishi T., Iwata T., et al., 1993, AJ 105, 1487
Eiroa C., Lenzen R., Miranda L.F., et al., 1993, AJ 106, 613
Eiroa C., Miranda L.F., Anglada G., Estalella R., Torrelles J.M., 1994a, A&A 283, 973
Eiroa C., Torrelles J.M., Miranda L.F., Anglada G., Estalella R., 1994b, A&AS 108, 73
Edwards S., Snell R.L., 1982, ApJ 261, 151
Edwards S., Snell R.L., 1984, ApJ 281, 237
Elias J.H., 1978, ApJ 224, 857
Felli M., Palagi F., Tofani G., 1992, A&A 255, 293
Frerking M.A., Langer W.D., 1982, ApJ 256, 523
Fukui Y., 1989, in Low Mass Star Formation and Pre-Main Sequence Objects, Reipurth B. (ed.). Garching: ESO, p. 95
Fukui Y., Sugitani K., Takaba H., et al., 1986, ApJ 311, L85
Fukui Y., Takaba H., Iwata T., Mizuno A., 1988, ApJ 325, L13
Fukui Y., Iwata T., Mizuno A., Bally J., Lane P., 1993, in Protostars and Planets III, Levy E.H. & Lunine J.I. (eds.). Tucson: Univ. of Arizona Press, p. 603
Fuller G.A., Myers P.C., 1993, ApJ 418, 273
Fuller G.A., Lada E.A., Masson C.R., Myers P.C., 1995, ApJ 453, 754
Genzel R., Reid M.J., Moran J.M., Downes D., 1981, ApJ 286, 599
Goldsmith P.F., Snell R.L., Hemeon-Heyer M., Langer W.D., 1984, ApJ 286, 599
Goodman A.A., Benson P.C., Fuller G.A., Myers P.C., 1993, ApJ 406, 528
Gyulbudaghian A.L., Glushkov Yu.I., Denisyuk E.K., 1978, ApJ 224, L137
Gyulbudaghian A.L., Rodríguez L.F., Mendoza-Torres E., 1987, Rev. Mex. Astron. Astrofis. 15, 53
Haikala L.K., Laureijs R.J., 1989, A&A 223, 287
Haikala L.F., Miller M., Gierens K., Winnewisser G., 1991, in Molecular Clouds, James R.A. & Millar T.J. (eds.). Cambridge: Cambridge Univ. Press, p. 25
Harju J., Walmsley C.M., Wouterloot J.G.A., 1991, A&A 245, 643
Haro G., 1953, ApJ 117, 73
Haro G., 1959 (private communication to G.H. Herbig)
Herbig G.H., 1974, Lick Obs. Bull. No. 658
Herbig G.H., Jones B.F., 1983, AJ 88, 1040
Heyer M.H., Snell R.L., Goldsmith P.F., Myers P.C., 1987, ApJ 321, 370
Jones B.F., Cohen M., Sirk M., Jarret R., 1984, AJ 89, 1404
Kun M., Prusti T., 1993, A&A 272, 235
Lada C.J., 1985, ARA&A 23, 267
Ladd E.F., Adams F.D., Casey S., et al., 1991a, ApJ 366, 203

Ladd E.F., Adams F.D., Casey S., et al., 1991b, ApJ 382, 555
Lebrun F., 1986, ApJ 306, 16
Levreault R.M., 1985, Ph.D. Thesis, University of Texas at Austin
Levreault R.M., 1988, ApJS 67, 283
Little L.T., Bergman P., Cunningham C.T., et al., 1988, A&A 205, 129
Lynds B.T., 1962, ApJS 7, 1
Loren R.B., 1977, ApJ 218, 716
Loren R.B., 1981, ApJ 249, 550
Maddalena R.J., Morris M., 1987, ApJ 323, 179
Maddalena R.J., Morris M., Moscowitz J., Thaddeus P., 1986, ApJ 303, 375
Marraco H.G., Rydgren A.E., 1981, AJ 86, 62
McMullin J.P., Mundy L.G., Blake G.A., 1994, ApJ 137, 305
Molinari S., Liseau R., Lorenzetti D., 1993, A&AS 101, 59
Morata O., et al., 1996 (in preparation)
Morgan J.A., Bally J., 1991, ApJ 372, 505
Morgan J.A., Snell R.L., Strom K.M., 1990, ApJ 362, 274
Morgan J.A., Schloerb F.P., Snell R.L., Bally J., 1991, ApJ 376, 618
Mundt R., Fried J.W., 1983, ApJ 274, L83
Mundt R., Bührke T., Fried J.W., et al., 1984, A&A 140, 17
Mundt R., Brugel E.W., Bührke T., 1987, ApJ 319, 275
Mundt R., Ray T.P., Bührke T., 1988, ApJ 333, L69
Mundy L.G., McMullin J.P., Grossman A.W., Sandell G., 1993, Icarus 106, 11
Myers P.C., Heyer M., Snell R.L., Goldsmith P.F., 1988, ApJ 324, 907
Myers P.C., Fuller G.A., Goodman A.A., Benson P.J., 1991, ApJ 376, 561
Myers P.C., Bachiller R., Caselli P., et al., 1995, ApJ 449, L65
Nakano M., Sugitani K., Sato F., Ogura K., 1994, ApJ 423, L147
Odenwald S.F., Schwartz P.R., 1993, ApJ 405, 706
Ogura K. 1985, in IAU Symp. 115, Star Forming Regions, Peimbert M. & Jugaku J. (eds.). Dordrecht: Reidel, p. 341
Ogura K., Walsch J.R., 1991, AJ 101, 185
Olberg M., Reipurth B., Booth R.S., 1989, in The Physics and Chemistry of Interstellar Molecular Clouds, Winnewisser G. & Armstrong J.T. (eds.) Lect. Notes Phys. 331, 120
Palla F., Brand J., Cesaroni R., Comoretto G., Felli M., 1991, A&A 246, 249
Parker N.D., 1991, MNRAS 251, 6
Parker N.D., Padman R., Scott P.F., Hills R.E., 1988, MNRAS 234, L67
Parker N.D., Padman, Scott P.F., 1991, MNRAS 252, 442
Pastor J., Estalella R., López R., et al., 1991, A&A 252, 320
Pauls T.A., Wilson T.L., Bieging J.H., Martin R.N., 1983, A&A 124, 23
Persi P., Ferrari-Toniolo M., Marenzi A.R., et al., 1994, A&A 282, 233
Petterson B., 1984, A&A 117, 183
Pudritz R.E., 1988, in Galactic and Extragalactic Star Formation, Pudritz R.E. & Fich M. (eds.). Dordrecht: Kluwer, p. 135
Pudritz R.E., Norman C.A., 1983, ApJ 274, 677
Raga A.C., Cantó J., Calvet N., Rodríguez L.F., Torrelles J.M., 1993, A&A 276, 539
Ray T.P., 1987, A&A 171, 145
Ray T.P., Poetzel R., Solf J., Mundt R., 1990, ApJ 357, L45
Reipurth B., 1985, A&AS 61, 319
Reipurth B., 1989, A&A 220, 249
Reipurth B., 1991, in The Physics of Star Formation and Early Stellar Evolution, Lada C.J. & Kylafis N.D. (eds.). Dordrecht: Kluwer, p. 497
Reipurth B., 1994, A general catalogue of Herbig-Haro objects, electronically published via anon. ftp to ftp.hq.eso.org, directory /pub/Catalogs/Herbig-Haro
Reipurth B., Gee G., 1986, A&A 166, 148
Reipurth B., Bally J., Graham J.A., Lane A., Zealey W.J., 1986, A&A 164, 51
Reipurth B., Chini R., Krugel E., Kreysa E., Sievers A., 1993, A&A 273, 221
Rodríguez L.F., 1990, in The Evolution of the Interstellar Medium, Blitz L. (ed.), ASP Conf. Ser. 12, 183
Rodríguez L.F., Carral P., Ho P.T.P., Moran J.M., 1982, ApJ 260, 635
Rodríguez L.F., Reipurth B., 1994, A&A 281, 882
Sato F., Fukui Y., 1989, ApJ 343, 773
Sato F., Mizuno A., Nagahama T., et al., 1994, ApJ 435, 279
Schwartz P.R., Gee G., Huang Y.-L., 1988, ApJ 327, 350
Snell R.L., Edwards S., 1982, ApJ 259, 668
Snell R.L., Loren R.B., Plambeck R.L., 1980, ApJ 239, L17
Snell R.L., Scoville N.Z., Sanders D.B., Erickson N.R., 1984, ApJ 284, 176
Smith H.A., Fischer J., Mozurkewich D., Schwartz P., 1989, Bull. AAS 20, 1093
Strom S.E., Grasdalen G.L., Strom K.M., 1974, ApJ 191, 111
Strom K.M., Strom S.E., Wolff S.C., Morgan J., Wenz M., 1986, ApJS 62, 39
Strom K.M., Newton G., Strom S.E., et al., 1989a, ApJS 71, 183
Strom K.M., Margulis M., Strom S.E., 1989b, ApJ 345, L79
Strom K.M., Margulis M., Strom S.E., 1989c, ApJ 346, L33
Tafalla M., Myers P.C., Wilner D.J., 1994, in Clouds, Cores and Low Mass Stars, Clemens D. and Barvainis R. (eds.) ASP Conf. Ser. 65, 391
Takaba H., Fukui Y., Fujimoto Y., et al., 1986, A&A 166, 276
Terebey S., Vogel S.N., Myers P.C., 1989, ApJ 340, 472
Torrelles J.M., Rodríguez L.F., Cantó J., et al., 1983, ApJ 274, 214
Uchida Y., Shibata K., 1985, PASJ 37, 515
Ungerechts H., Walmsley C.M., Winnewisser G., 1986, A&A 157, 207
Verdes-Montenegro L., Torrelles J.M., Rodríguez L.F., et al., 1989, ApJ 346, 193
Vrba F.J., Luginbuhl C.B., Strom S.E., Strom K.M., Heyer M.H., 1986, AJ 92, 633
Weintraub D.A., 1990, ApJS 74, 575
Wilking B.A., Mundy L.G., Blackwell J.H., Howe J.E., 1989, ApJ 345, 257
Wilking B.A., Blackwell J.H., Mundy L.G., 1990, AJ 100, 758
Wilking B.A., Claussen M.J., Benson P.J., et al., 1994, ApJ 431, L119
Xiang D., Turner B.E., 1995, ApJS 99, 121
Yun J.L., Clemens D.P., 1994, ApJS 92, 145
Zhou S., Wu Y., Evans N.J., et al., 1989, ApJ 346, 168